
Efficient Discretizations of Optimal Transport

Junqi Wang¹ Pei Wang¹ Patrick Shafto¹

Abstract

Obtaining solutions to Optimal Transportation (OT) problems is typically intractable when the marginal spaces are continuous. Recent research has focused on approximating continuous solutions with discretization methods based on i.i.d. sampling, and has proven convergence as the sample size increases. However, obtaining OT solutions with large sample sizes requires intensive computation effort, that can be prohibitive in practice. In this paper, we propose an algorithm for calculating discretizations with a given number of points for marginal distributions, by minimizing the (entropy-regularized) Wasserstein distance, and result in plans that are comparable to those obtained with much larger numbers of i.i.d. samples. Moreover, a local version of such discretizations which is parallelizable for large scale applications is proposed. We prove bounds for our approximation and demonstrate performance on a wide range of problems.

1. Introduction

Optimal transport is the problem of finding a coupling of probability distributions that minimizes cost (Kantorovich, 2006), and is a technique applied across various fields and literatures (Peyré & Cuturi, 2019; Villani, 2008). Although many methods exist for obtaining optimal transference plans for distributions on discrete spaces, computing the plans is not generally possible for continuous spaces (Janati et al., 2020). Given the prevalence of continuous spaces in machine learning, this is a significant limitation for theoretical and practical applications.

One strategy for approximating continuous OT plans is based on discrete approximation, e.g. via samples. Recent research has provided guarantees on the fidelity of discrete, sample-based approximations to continuous OT as $N \rightarrow \infty$

(Aude et al., 2016). Specifically, by sampling large numbers of points S_i from each marginal, one may compute discrete optimal transference plan on $S_1 \times S_2$, with the cost matrix being derived from pointwise evaluation of the cost function on $S_1 \times S_2$.

Even in the discrete case, obtaining minimal cost plans is computationally challenging. For example, Sinkhorn scaling, which computes an entropy-regularized approximation to OT plans, has a complexity that scales with $|S_1 \times S_2|$ (Allen-Zhu et al., 2017). Though many comparable methods exist (Lin et al., 2019), all have complexity that scales with the product of sample sizes, and require construction of the cost matrix that also scales with $|S_1 \times S_2|$.

Building on previous sample-based approaches, we develop methods for optimizing small N approximations of OT plans. In Sec. 2, we formulate the problem of fixed size approximation and reduce it to discretization problems on marginals with theoretical guarantees. In Sec. 3, the gradient of entropy-regularized Wasserstein distance between a continuous distribution and its discretization is calculated. In Sec. 4, we present a stochastic gradient descent algorithm that is based on optimization of the location and weight of the points with empirical test results. Sec. 5 introduces parallelizable algorithm via decompositions of the marginal spaces, which can exploit the intrinsic geometry. In Sec. 6, we analyze time and space complexity, and provide comparison with the naive sampling.

2. Optimal Discretizations

Let (X, d_X) , (Y, d_Y) be compact Polish spaces (complete separable metric spaces), $\mu \in \mathcal{P}(X)$, $\nu \in \mathcal{P}(Y)$ be probability distributions on their Borel-algebras, and $c : X \times Y \rightarrow \mathbb{R}$ be a cost function. Denote the set of all joint probability measures on $X \times Y$ with marginals μ and ν by $\Pi(\mu, \nu)$. For a given cost function c , the *optimal transference (OT) plan* between μ and ν is defined as (Kantorovich, 2006):

$$\gamma(\mu, \nu) := \operatorname{argmin}_{\pi \in \Pi(\mu, \nu)} \langle c, \pi \rangle$$

where $\langle c, \pi \rangle := \int_{X \times Y} c(x, y) d\pi(x, y)$.

When $X = Y$, if cost $c(x, y) = d_X^k(x, y)$, $W_k(\mu, \nu) = \langle c, \gamma(\mu, \nu) \rangle^{1/k}$ defines the k -Wasserstein distance between μ and ν for $k \geq 1$. Here $d_X^k(x, y)$ is the k -th power of the

¹Department of Mathematics & Computer Science, Rutgers University, Newark, US. Correspondence to: Pei Wang <pei.wang@rutgers.edu>.

Preliminary work. Under review by the International Conference on Machine Learning (ICML). Do not distribute.

metric d_X on X .

Entropy regularized optimal transport (EOT) (Cuturi, 2013; Aude et al., 2016) was introduced to ease the computational burden of obtaining OT plan:

$$\gamma_\lambda(\mu, \nu) := \operatorname{argmin}_{\pi \in \Pi(\mu, \nu)} \langle c, \pi \rangle + \lambda \operatorname{KL}(\pi \| \mu \otimes \nu) \quad (1)$$

where $\lambda > 0$ is a regularization parameter and $\operatorname{KL}(\pi \| \mu \otimes \nu) := \int \log\left(\frac{d\pi}{d\mu \otimes d\nu}\right) d\pi$ is the Kullback-Leibler divergence. EOT smooths the classical OT into a convex problem. Hence, given (μ, ν, c) , there exists a unique solution to (1). After X and Y are discretized, EOT problems can be solved by Sinkhorn iteration (Sinkhorn & Knopp, 1967), which can be easily parallelized. However, for large-scale discrete spaces, the computational cost can still be unfeasible (Allen-Zhu et al., 2017). Even worse, to even apply Sinkhorn iteration, one must have a cost matrix, which itself can be a non-trivial computational burden to obtain; in some cases, for example where the cost is derived from a probability model (Wang et al., 2020a), it may require intractable computations (Tran et al., 2017; Overstall et al., 2020).

We propose to efficiently estimate continuous OT with a fixed size discrete approximation. In more details, let $m, n \in \mathbb{Z}^*$, $\mu_m \in \mathcal{P}(X)$, $\nu_n \in \mathcal{P}(Y)$ be discrete approximation of μ, ν respectively with $\mu_m = \sum_{i=1}^m w_i \delta_{x_i}$ and $\nu_n = \sum_{j=1}^n u_j \delta_{y_j}$, $x_i \in X$, $y_j \in Y$ and $w_i, u_j \in \mathbb{R}^+$. Then the EOT plan $\gamma_\lambda(\mu, \nu) \in \Pi(\mu, \nu)$ for OT problem (μ, ν, c) , can be approximated by the EOT plan $\gamma_\lambda(\mu_m, \nu_n) \in \Pi(\mu_m, \nu_n)$ for OT problem (μ_m, ν_n, c) .

To obtain the best estimation the OT problem of (μ, ν, c) with fixed size $m, n \in \mathbb{Z}^*$, we introduce the objective:

$$\Omega_{k,\rho}(\mu_m, \nu_n) = W_k^k(\mu, \mu_m) + W_k^k(\nu, \nu_n) + \rho W_k^k(\gamma_\lambda(\mu, \nu), \gamma_\lambda(\mu_m, \nu_n)), \quad (2)$$

$W_k^k(\mu, \mu_m)$, $W_k^k(\nu, \nu_n)$ and $W_k^k(\gamma_\lambda(\mu, \nu), \gamma_\lambda(\mu_m, \nu_n))$ are the k -th power of k -Wasserstein distances between $\mu, \nu, \gamma_\lambda(\mu, \nu)$ and their approximations $\mu_m, \nu_n, \gamma_\lambda(\mu_m, \nu_n)$. The hyperparameter $\rho > 0$ balances between the estimation accuracy over marginals and that of the transference plan.

To properly compute $W_k^k(\gamma_\lambda(\mu, \nu), \gamma_\lambda(\mu_m, \nu_n))$, a metric $d_{X \times Y}$ on $X \times Y$ is needed. Without loss of generality, we assume there exists a constant A such that

$$\max\{d_X^k(x_1, x_2), d_Y^k(y_1, y_2)\} \stackrel{(i)}{\leq} d_{X \times Y}^k((x_1, y_1), (x_2, y_2)) \stackrel{(ii)}{\leq} A(d_X^k(x_1, x_2) + d_Y^k(y_1, y_2)). \quad (3)$$

For instance, (3) holds when $d_{X \times Y}$ is the p -product metric for $1 \leq p \leq \infty$. In particular, when $p = k = 1$, the equality

holds at (ii) with $A = 1$; when $d_{X \times Y}$ is the ∞ -product metric, equality holds at (i).

To efficiently compute (2), three Wasserstein distances are estimated by their entropy regularized approximations (Luise et al., 2018):

$$\Omega_{k,\zeta,\rho}(\mu_m, \nu_n) = W_{k,\zeta}^k(\mu, \mu_m) + W_{k,\zeta}^k(\nu, \nu_n) + \rho W_{k,\zeta}^k(\gamma_\lambda(\mu, \nu), \gamma_\lambda(\mu_m, \nu_n)). \quad (4)$$

For instance, $W_k^k(\mu, \mu_m) = \langle d_X^k, \gamma(\mu, \mu_m) \rangle^{1/k}$ is estimated by $W_{k,\zeta}^k(\mu, \mu_m) = \langle d_X^k, \gamma_\zeta(\mu, \mu_m) \rangle^{1/k}$ with regularizer ζ . Here $\gamma_\zeta(\mu, \mu_m)$ is computed by optimizing:

$$\widehat{W}_{k,\zeta}^k(\mu, \mu_m) = \langle d_X^k, \gamma_\zeta(\mu, \mu_m) \rangle + \lambda \operatorname{KL}(\gamma_\zeta(\mu, \mu_m) \| \mu \otimes \mu_m).$$

A major drawback of optimizing $\Omega_{k,\zeta,\rho}(\mu_m, \nu_n)$ is evaluating the Wasserstein distance between $\gamma_\lambda(\mu, \nu)$ and $\gamma_\lambda(\mu_m, \nu_n)$. In fact, calculating $\gamma_\lambda(\mu, \nu)$ is intractable, which is the original motivation to compute $\gamma_\lambda(\mu_m, \nu_n)$. To overcome this difficulty, utilizing the dual formulation of the entropy regularized OT, we show that ¹:

Proposition 2.1. *When X and Y are two compact spaces and c is \mathcal{C}^∞ , there exists a constant $C_1 \in \mathbb{R}^+$ such that*

$$\max\{W_k^k(\mu, \mu_m), W_k^k(\nu, \nu_n)\} \leq W_{k,\zeta}^k(\gamma_\lambda(\mu, \nu), \gamma_\lambda(\mu_m, \nu_n)) \leq C_1 [W_{k,\zeta}^k(\mu, \mu_m) + W_{k,\zeta}^k(\nu, \nu_n)]. \quad (5)$$

Proposition 2.1 indicates that $\Omega_{k,\zeta,\rho}(\mu_m, \nu_n)$ can be approximated by $W_{k,\zeta}^k(\mu, \mu_m) + W_{k,\zeta}^k(\nu, \nu_n)$. Thus when the continuous marginals μ and ν are properly approximated, so is the optimal transference plan between them. Therefore, in the next sections, we will focus on developing algorithms to obtain μ_m^*, ν_n^* that minimize $W_{k,\zeta}^k(\mu, \mu_m)$ and $W_{k,\zeta}^k(\nu, \nu_n)$.

3. Gradient of the Objective Function

Let $\nu = \sum_{i=1}^m w_i \delta_{y_i}$ be the discrete probability measure in position of “ μ_m ” in the last section. The task now is to minimize $W_{k,\zeta}^k(\mu, \nu)$ about the target discrete probability measure ν on X , where μ is a fixed continuous probability measure on X . The entropy-approximated Wasserstein $W_{k,\zeta}^k(\mu, \nu)$ is convex on w_i ’s, while its “convexity” on y_i ’s are not defined for a general X .

In this section, we derive the gradient of $W_{k,\zeta}^k(\mu, \nu)$ about ν following the discrete discussions of (Wang et al., 2020b; Luise et al., 2018), for applying stochastic gradient descent (SGD) on both the positions $\{y_i\}_{i=1}^m$ and their weights $\{w_i\}_{i=1}^m$. The SGD on X is either through an exponential map, or by treating X as (part of) an Euclidean space.

¹Proofs are included in the Supplementary Material.

Let $g(x, y) := d_X^k(x, y)$, and denote the joint distribution minimizing $\widehat{W}_{k, \zeta}^k$ as π with differential form at (x, y_i) being $d\pi_i(x)$, which is used to define $W_{k, \zeta}^k$ in Section 2.

By introducing Lagrange multipliers $\alpha \in L^\infty(X)$, $\beta \in \mathbb{R}^m$, $\widehat{W}_{k, \zeta}^k(\mu, \nu) = \max_{\alpha, \beta} \mathcal{L}(\mu, \nu; \alpha, \beta)$ where $\mathcal{L}(\mu, \nu; \alpha, \beta) = \int_X \alpha(x) d\mu(x) + \sum_{i=1}^n \beta w_i - \zeta \int_X \sum_{i=1}^n w_i E_i(x) d\mu(x)$ with $E_i(x) = e^{(\alpha(x) + \beta_i g(x, y_i)) / \zeta}$ (See (Aude et al., 2016) or Supplementary). Let α^*, β^* be the argmax, we have

$$W_{k, \zeta}^k(\mu, \nu) = \int_X \sum_{i=1}^n g(x, y_i) E_i^*(x) w_i d\mu(x)$$

with $E_i^*(x) = e^{(\alpha^*(x) + \beta_i^* - g(x, y_i)) / \zeta}$. Since $\alpha'(x) := \alpha(x) + t$ and $\beta'_i := \beta_i - t$ produces the same $E_i(x)$ for any $t \in \mathbb{R}$, the representative with $\beta_n = 0$ that is equivalent to β (as well as β^*) is denoted by $\bar{\beta}$ (similarly $\bar{\beta}^*$) below, in order to get uniqueness, making the differentiation possible.

From a direct differentiation of $W_{k, \zeta}^k$, we have

$$\begin{aligned} \frac{\partial W_{k, \zeta}^k}{\partial w_i} &= \int_X g(x, y_i) E_i^*(x) d\mu(x) + \\ &\frac{1}{\zeta} \int_X \sum_{j=1}^n g(x, y_j) \left(\frac{\partial \alpha^*(x)}{\partial w_i} + \frac{\partial \beta_j^*}{\partial w_i} \right) w_j E_j^*(x) d\mu(x). \end{aligned} \quad (6)$$

$$\begin{aligned} \nabla_{y_i} W_{k, \zeta}^k &= \int_X \nabla_{y_i} g(x, y_i) \left(1 - \frac{g(x, y_i)}{\zeta} \right) E_i^*(x) w_i d\mu(x) + \\ &\frac{1}{\zeta} \int_X \sum_{j=1}^n g(x, y_j) (\nabla_{y_i} \alpha^*(x) + \nabla_{y_i} \beta_j^*) w_j E_j^*(x) d\mu(x). \end{aligned} \quad (7)$$

With the transference plan $d\pi_i(x) = w_i E_i^*(x) d\mu(x)$ and the derivatives of $\alpha^*, \beta^*, g(x, y_i)$ calculated, the gradient of $W_{k, \zeta}^k$ can be assembled.

Assume that g is Lipschitz and is differentiable almost everywhere (for $k \geq 1$, and d_X Euclidean distance in \mathbb{R}^d , differentiability fails to hold only when $k = 1$ and $y_i = x$), and that $\nabla_y g(x, y)$ is calculated. The derivatives of α^* and $\bar{\beta}^*$ can then be calculated thanks to Implicit Function Theorem for Banach spaces (see (Accinelli, 2009)).

The maximality of \mathcal{L} at α^* and $\bar{\beta}^*$ induces that $\mathcal{N} := \nabla_{\alpha, \bar{\beta}} \mathcal{L}|_{(\alpha^*, \bar{\beta}^*)} = 0 \in (L^\infty(X) \otimes \mathbb{R}^{m-1})^\vee$, the Fréchet derivative vanishes. Differentiate (in the sense of Fréchet) again on $(\alpha, \bar{\beta})$ and y_i, w_i , respectively, we get

$$\nabla_{(\alpha, \bar{\beta})} \mathcal{N} = -\frac{1}{\zeta} \begin{bmatrix} d\mu(x) \delta(x, x') & d\pi_j(x') \\ d\pi_i(x) & w_i \delta_{ij} \end{bmatrix} \quad (8)$$

as a bilinear functional on $L^\infty(X) \times \mathbb{R}^{m-1}$ (note that in Eq. (8), the index i of $d\pi_i$ cannot be m). The bilinear functional $\nabla_{(\alpha, \bar{\beta})} \mathcal{N}$ is invertible, and denote its inverse by \mathbf{M} as a bilinear form on $(L^\infty(X) \otimes \mathbb{R}^{m-1})^\vee$.

The last ingredient for Implicit Function Theorem is $\nabla_{w_i, y_i} \mathcal{N}$:

$$\nabla_{w_i} \mathcal{N} = \left(-\frac{1}{w_i} \int_X (\cdot) d\pi_i(x), \vec{0} \right) \quad (9)$$

$$\begin{aligned} \nabla_{y_i} \mathcal{N} &= \left(\frac{1}{\zeta} \int_X (\cdot) \nabla_{y_i} g(x, y_i) d\pi_i(x), \right. \\ &\left. \frac{\delta_{ij}}{\zeta} \int_X \nabla_{y_i} g(x, y_i) d\pi_i(x) \right). \end{aligned} \quad (10)$$

Then $\nabla_{w_i, y_i}(\alpha^*, \bar{\beta}^*) = \mathbf{M}(\nabla_{w_i, y_i} \mathcal{N})$.

Therefore, we have gradient $\nabla_{w_i, y_i} W_{k, \zeta}^k$ calculated.

Moreover, we can differentiate Eq. (6), (7), (8), (9), (10) to get a Hessian matrix of $W_{k, \zeta}^k$ on w_i 's and y_i 's provided a better differentiability of $g(x, y)$ (which may enable Newton's method, or a mixture of Newton's method and minibatch SGD to accelerate the convergence). More details about claims, calculations and proofs are provided in the Supplementary Text.

4. The Discretization Algorithm

Here we provide a description of an algorithm for Efficient Discretizations of Optimal Transport (EDOT) from a distribution μ to μ_m with integer m , a given cardinality of support. In general, μ need not be explicitly accessible, and even if it is accessible, exactly computing the transference plan is not feasible. Therefore, in this construction, we assume μ is given in terms of a **random sampler**, and apply minibatch stochastic gradient descent (SGD) through a set of samples independently drawn from μ of size N on each step to approximate μ .

Recall that to calculate the gradient $\nabla_{\mu_m} W_{k, \zeta}^k(\mu, \mu_m) = \left(\nabla_{x_i} W_{k, \zeta}^k(\mu, \mu_m), \nabla_{w_i} W_{k, \zeta}^k(\mu, \mu_m) \right)_{i=1}^m$, we need

- 1). $\pi_{X, \zeta}$, the EOT transference plan between μ and μ_m ,
- 2). the cost $g = d_X^k$ on X and, 3). its gradient on the second variable $\nabla_{x'} d_X^k(x, x')$. From N samples $\{y_i\}_{i=1}^N$, we can construct $\mu_N = \frac{1}{N} \sum_{i=1}^N \delta_{y_i}$ and calculate the gradients with μ replaced by μ_N as an estimation, whose effectiveness (convergence as $N \rightarrow \infty$) is induced by (Aude et al., 2016). The algorithm is stated in Algorithm 1 (EDOT).

In simulations, we choose $k = 2$ to reduce complexity in calculating the distance function (square of Euclidean distance is quadratic) and its derivatives. The regularizer ζ should be small enough to reduce the error of the EOT estimation $W_{k, \zeta}^k$ of the Wasserstein distance W_k . However, setting ζ too small will make $e^{-g(x, y) / \zeta}$ or its byproduct in Sinkhorn algorithm indistinguishable from 0 in *double*

format. Our strategy is setting $\zeta = 0.01$ for X of diameter 1 and scales proportional with $\text{diam}(X)^k$ (see next section).

Algorithm 1 Simple EDOT using minibatch SGD

input: μ, k, m, ζ, N batch size, ϵ for stopping criterion, $\alpha = 0.2$ for momentum, $\beta = 0.2$ for learning rate.

output: $x_i \in X, w_i > 0$ such that $\mu_m = \sum_{i=1}^m w_i \delta_{x_i}$.

initialize: randomly choose $\sum_{i=1}^m w_i^{(0)} \delta_{x_i^{(0)}}$; set $t = 0$;

 set learning rate $\eta_t = 0.5(1 + \beta t)^{-1/2}$ (for $t > 0$).

repeat

 Set $t \leftarrow t + 1$;

 Sample N points $\{y_j\}_{j=1}^N \subseteq X$ from μ independently;

 Construct $\mu_N^{(t)} = \frac{1}{N} \sum_{j=1}^N \delta_{y_j}$;

 Calculate gradients $\nabla_{\mathbf{x}} \widehat{W}_{k,\zeta}^k(\mu_N^{(t)}, \mu_m^{(t)})$ and

$$\nabla_{\mathbf{w}} \widehat{W}_{k,\zeta}^k(\mu_N^{(t)}, \mu_m^{(t)});$$

 Update $D\mathbf{x}_t \leftarrow \alpha D\mathbf{x}_{t-1} + \nabla_{\mathbf{x}} \widehat{W}_{k,\zeta}^k(\mu_N^{(t)}, \mu_m^{(t)})$,

$$D\mathbf{w}_t \leftarrow \alpha D\mathbf{w}_{t-1} + \nabla_{\mathbf{w}} \widehat{W}_{k,\zeta}^k(\mu_N^{(t)}, \mu_m^{(t)});$$

 Update $\mathbf{x}^{(t)} \leftarrow \mathbf{x}^{(t-1)} - \eta_t D\mathbf{x}_t$,

$$\mathbf{w}^{(t)} \leftarrow \mathbf{w}^{(t-1)} - \eta_t D\mathbf{w}_t;$$

until $|\nabla_{\mathbf{x}} \widehat{W}_{k,\zeta}^k| + |\nabla_{\mathbf{w}} \widehat{W}_{k,\zeta}^k| < \epsilon$;

 Set output $x_i \leftarrow x_i^{(t)}, w_i \leftarrow w_i^{(t)}$.

4.1. Examples of Discretization

We demonstrate our algorithm on: **1).** μ is the uniform distribution on $X = [0, 1]$. **2).** μ is the mixture of two truncated normal distributions on $X = [0, 1]$, the PDF is $f(x) = 0.3\phi(x; 0.2, 0.1) + 0.7\phi(x; 0.7, 0.2)$, where $\phi(x; \xi, \sigma)$ is the density of the truncated normal distribution on $[0, 1]$ with expectation ξ and standard deviation σ . **3).** μ is the mixture of two truncated normal distributions on $X = [0, 1]^2$, the two distributions are: $\phi(x; 0.2, 0.1)\phi(y; 0.3, 0.2)$ of weight 0.3 and $\phi(x; 0.7, 0.2)\phi(y; 0.6, 0.15)$ of weight 0.7.

Let $k = 2, \zeta = 0.01, N = 100$ for all plots in this section. Fig. 1 (1-3) plot the discretizations (μ_m) for example (1-3) with $m = 5, 5, 7$ respectively.

Convergence. There is no guarantee that Algorithm 1 converges to the global optimal positions (though if stabilized at some positions, the weights are optimized). On these examples we usually iterate 5000 to 6000 steps to get a result (gradients will be small, but are still affected by the fluctuation caused by the sample size N). We estimate entropy-regularized Wasserstein $W_{k,\zeta}^k$ between μ and μ_m by Richardson extrapolation (see Supplementary for details) and use it to score the convergence rate.

Fig. 1 (6) illustrates the convergence rate of $W_{k,\zeta}^k(\mu, \mu_m)$ versus SGD steps on example 2 (1D truncated normal mixture) with μ_m obtained by 5-point EDOT.

Generally, Wasserstein distance decays and gets close to final state after tens of steps, while slight changes can still be observed (in 1D examples) even after 3000 steps. Some-

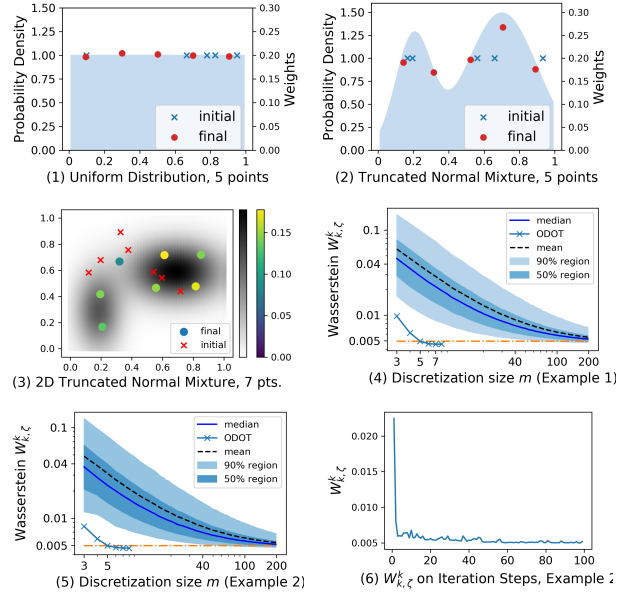


Figure 1. (1-3) plot sample discretizations of the examples (1-3). In (3), x -axis and y -axis are the 2D coordinates, the probability density of μ and weights of μ_m are encoded by color. (4,5) Comparisons with i.i.d. sampling on Wasserstein distance to the continuous distribution. EDOT are calculated with $m = 3$ to 7 (3 to 8). The 4 boundary curves of the shaded region are 5%-, 25%-, 75%- and 95%-percentile curves, orange line represents the level of $m = 5$; (6) plots the entropy regularized Wasserstein distance $W_{k,\zeta}^k(\mu, \mu_m)$ versus SGD steps on example 2 (1D truncated normal mixture) with μ_m optimized by 5-point EDOT.

times an ill positioned initial distribution can make it slower to approach a stationary state.

Comparison with Naive Sampling. Fig. 1 (4-5) plot the entropy-regularized Wasserstein $W_{k,\zeta}^k(\mu, \mu_m)$ with different choices of m for Example 1) and 2). Here μ_m 's are generated by two methods: a). Algorithm 1 with m chosen from 3 to 7 in Example 1 and to 8 in Example 2, shown by \times 's. b). naive sampling (i.i.d. with equal weights) simulated using Monte Carlo of volume 20000 on each size from 3 to 200. Fig. 1 (4-5) demonstrate the effectiveness of EDOT: as indicated by the orange horizontal dashed line, even 5 points in these 2 examples excels 95% of naive samplings of size 40 and 75% of naive samplings of size over 100.

4.2. An Example on Transference Plan

In Fig. 2, we illustrate an application of EDOT on an optimal transport task as proposed in Section 2. The optimal transport problem has $X = Y = [0, 1]$, and the marginal distributions μ, ν are truncated normal (mixtures), where μ has 2 components (shown on the left) and ν has only 1 component (shown on the top). The cost function is taken as the square of Euclidean distance on an interval. We can see

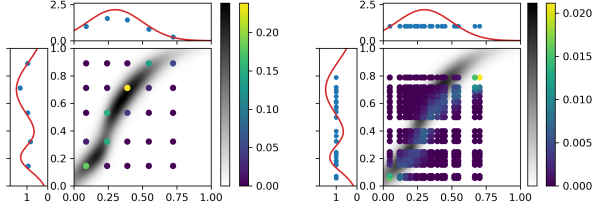


Figure 2. Approximation of the transference plan. Left: EDOT on 5×5 grid with $W_{k,\zeta}^k(\mu, \mu_5) = 4.792 \times 10^{-3}$, $W_{k,\zeta}^k(\nu, \nu_5) = 5.034 \times 10^{-3}$, $W_{k,\zeta}^k(\gamma, \gamma_{5,5}) = 8.446 \times 10^{-3}$; Right: Naive on 25×25 grid with $W_{k,\zeta}^k(\mu, \mu_7) = 5.089 \times 10^{-3}$, $W_{k,\zeta}^k(\nu, \nu_7) = 2.222 \times 10^{-2}$, $W_{k,\zeta}^k(\gamma, \gamma_{7,7}) = 2.563 \times 10^{-2}$. In both figures, the background grayscale density represents the true EOT density.

that on the 5×5 EDOT example, the high density area of the transference plan are correctly covered by lattice points with high weights, while in the naive sampling, even in grid size 25×25 , the points on the lattice with highest weights missed the region where true transference plan is of the most density. Comparison on Wasserstein distance also tells us EDOT works better with a smaller grid.

5. Methods of Improvement

5.1. Adaptive Cell Refinement

The computational cost of simple EDOT increases with the dimensionality and diameter of the underlying space. Larger m discretization $\mu_m = \sum_{i=1}^m w_i \delta_{y_i}$ is needed to capture the higher dimensional distributions. This will result an increase in parameters in SGD for calculating the gradient of $W_{k,\zeta}^k$: md for positions y_i 's and $m - 1$ for weights w_i 's. Such an increment will both increase complexity in each step, and also require more steps for SGD to converge. Furthermore, the calculation will have a higher complexity ($\mathcal{O}(mN)$) for each normalization in Sinkhorn.

We propose to reduce computational complexity by “divide and conquer”. The Wasserstein distance takes k -th power of the distance function d_X^k as cost function. The locality of distance d_X makes the solution to the OT / EOT problem local, meaning the probability mass is more likely to be transported to a close destination than to a remote one. Thus we can “divide and conquer” — cut the space X into small cells and solve the discretization problem separately. We require an adaptive dividing procedure to balance the accuracy and computational intensity among the cells. Therefore, determining size of discretization and choosing a proper regularizer for each cell are questions to answer, after having a partition $X = X_1 \sqcup \dots \sqcup X_{\mathcal{I}}$. We first sample a large sample set $S \sim \mu$ (with $|S| \gg N$) and partition S into $S_1 \sqcup \dots \sqcup S_{\mathcal{I}}$ according to X . In other words, to construct an EDOT problem for each X_i and sample set S_i located in X_i , we must figure out the parameters m_i and ζ_i .

Choosing Size m . An appropriate choice of m_i will balance contributions to the Wasserstein among the subproblems as follows: Let X_i be a manifold of dimension d , let $\text{diam}(X_i)$ be its diameter, and $p_i = \mu(X_i)$ be the probability of X_i . The entropy regularized wasserstein distance can be estimated as $W_{k,\zeta}^k = \mathcal{O}(p_i m_i^{-k/d} \text{diam}(X_i)^k)$ (Weed et al., 2019; Dudley, 1969). The contribution to $W_{k,\zeta}^k(\mu, \mu_m)$ per point in support of μ_m is $\mathcal{O}(p_i m_i^{-(k+d)/d} \text{diam}(X_i)^k)$. Therefore, to balance each point’s contribution to the Wasserstein among the divided subproblems, we set $m_i \approx \frac{(p_i \text{diam}(X_i)^k)^{d/(k+d)}}{\sum_{j=1}^{\mathcal{I}} (p_j \text{diam}(X_j)^k)^{d/(k+d)}}$. Since m_i must be an integer, it is rounded properly. If some cell has $m_i = 0$, then the probability should be added to its adjacent cells.²

Adjusting Regularizer ζ . In the calculation of $W_{k,\zeta}^k$, the Sinkhorn iterations on $e^{-g(x,y)/\zeta}$ is calculated. Therefore, ζ should scale with $g(x, y)$ (i.e., d_X^k) to make the transference plan not be affected by scaling of d_X . Precisely, we may choose $\zeta_i = \text{diam}(X_i)^k \zeta_0$ for some constant ζ_0 .

The Construction. Theoretically, the idea of division can be applied to any refinement procedure that can be applied iteratively and eventually makes the diameter of the cells approach 0. In our simulation, we use an adaptive kd-tree style cell refinement in an Euclidean space \mathbb{R}^d .

Let X be embedded into \mathbb{R}^d within an axis-aligned rectangular region. We choose an axis \mathbf{x}_l in \mathbb{R}^d and evenly split the region along a hyperplane orthogonal to \mathbf{x}_l (e.g. cut square $[0, 1]^2$ along the line $x = 0.5$), thus we construct X_1 and X_2 . With a sample set S given, we split it into two sample sizes S_1 and S_2 according to which subregion each sample is located in. Then the corresponding m_i and ζ_i can be calculated as discussed above. Thus two cells and corresponding subproblems are constructed. If some of the m_i is still too large, the cell is cut along another axis to construct two other cells. The full list of cells and subproblems can be constructed recursively, see Algorithm 2.

After having the set of subproblems, we may apply Algorithm 1 for solutions in each cell (samples used there are redrawn from the sample set S_i in each subproblem), then combine the solutions $\mu_{m_i}^{(i)} = \sum_{j=1}^{m_i} w_j^{(i)} \delta_{y_j^{(i)}}$ into the final result $\mu_m := \sum_{i=1}^{\mathcal{I}} \sum_{j=1}^{m_i} p_i w_j^{(i)} \delta_{y_j^{(i)}}$.

Fig. 3 shows the optimal discretization for the example in Fig. 1(3)) with $m = 30$, obtained by applying the EDOT with adaptive cell refinement.

²In general, there are various ways of distributing the probability to neighbors (in Algorithm 2, it is unique).

Algorithm 2 Adaptive Refinement via Depth First Search

input: m, μ, N_0 sample size, m_* max number of points in a cell, $\mathbf{a} = (a_0, a_1, \dots, a_{d-1})$ and $\mathbf{b} = (b_0, b_1, \dots, b_{d-1})$ as lower/upper bounds of the region;
output: *out*: stack of subproblems (S_i, m_i, p_i) with $\sum p_i = 1, \sum m_i = m, \sum |S_i| = N_0$;
initialization: $p_0 \leftarrow 1; T, out$ be empty stacks;
 Sample N_0 points $S_0 \sim \mu$;
 $T.push((S_0, m, p_0, \mathbf{a}, \mathbf{b}))$;
while T is not empty **do**
 $(S, m, p, \mathbf{a}, \mathbf{b}) \leftarrow T.pop()$;
 $l \leftarrow \operatorname{argmax} \{b_i - a_i\}, mid \leftarrow (a_l + b_l)/2$;
 $\mathbf{a}^{(1)} \leftarrow \mathbf{a}, \mathbf{a}^{(2)} \leftarrow (a_0, \dots, mid, \dots, a_{d-1})$;
 $\mathbf{b}^{(1)} \leftarrow (b_0, \dots, mid, \dots, b_{d-1}), \mathbf{b}^{(2)} \leftarrow \mathbf{b}$;
 $S_1 \leftarrow \{\mathbf{x} \in S : x_l \leq mid\}, S_2 \leftarrow \{\mathbf{x} \in S : x_l > mid\}$;
 $N_1 \leftarrow |S_1|, N_2 \leftarrow |S_2|$;
 $m_1 \leftarrow \operatorname{Round}_{0.5\uparrow} \left(\frac{N_1^{d/(k+d)}}{N_1^{d/(k+d)} + N_2^{d/(k+d)}} \right)$;
 $m_2 \leftarrow \operatorname{Round}_{0.5\downarrow} \left(\frac{N_2^{d/(k+d)}}{N_1^{d/(k+d)} + N_2^{d/(k+d)}} \right)$;
 if $m_1 = 0$ **then**
 $p_1 \leftarrow 0, p_2 \leftarrow (N_1 + N_2)/N_0$;
 else if $m_2 = 0$ **then**
 $p_1 \leftarrow (N_1 + N_2)/N_0, p_2 \leftarrow 0$;
 else
 $p_1 \leftarrow N_1/N_0, p_2 \leftarrow N_2/N_0$;
 end if
 for $i \leftarrow 1, 2$ **do**
 if $m_i > m_*$ **then**
 $T.push((S_i, m_i, p_i, \mathbf{a}^{(i)}, \mathbf{b}^{(i)}))$;
 else if $m_i > 0$ **then**
 $out.push((S_i, m_i, p_i))$;
 end if
 end for
end while

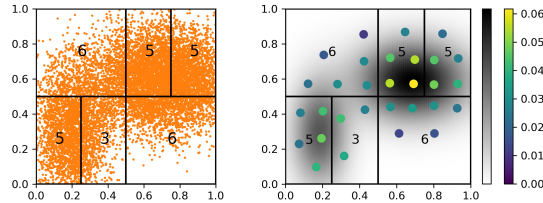


Figure 3. An example of adaptive refinement on a unit square. Left: division of 10000 sample S approximating a mixture of two truncated normal distributions, and the refinement for 30 discretization points. Right: the discretization optimized locally and combined as a probability measure, with $k = 2$.

5.2. On Embedded CW-Complexes

Although the samples on space X are usually represented as a vector in \mathbb{R}^d , inducing an embedding $X \hookrightarrow \mathbb{R}^d$, the space X usually has its own structure as a CW-complex (or simply a manifold) with a metric.

As the metric in the CW-complex usually bears a more intrinsic structure of X than the one induced by the embed-

ding, if the CW-complex structure and the metric is known, even piecewise, we may apply Algorithm 1 or Algorithm 2 on each cell or piece to get a precise discretization of X regarding its own metric, whereas direct discretization as a subset in \mathbb{R}^d may result in low expressing efficiency e.g. some points may drift off from X .

We show two examples: truncated normal mixture distribution on a Swiss roll, and a mixture normal distribution on a sphere mapped through stereographic projection.

On Swiss Roll. In this case, the underlying space X_{swiss} is a the Swiss Roll, a 2D rectangular strip embedded in \mathbb{R}^3 : $(\theta, z) \mapsto (\theta, \theta, z)$ in cylindrical coordinates, μ_{swiss} is a truncated normal mixture on (θ, z) -plane. Samples $S_{\text{swiss}} \sim \mu_{\text{swiss}}$ over X_{swiss} is shown on Fig. 4 (left) embedded in 3D and Fig. 5 (1) isometric into \mathbb{R}^2 .

Following the Euclidean metric in \mathbb{R}^3 , Fig. 4 (right) plots the EDOT solution μ_m through adaptive cell refinement (Algorithm 2) with $m = 50$. The resulting cell structure is shown as colored boxes. The corresponding partition of S_{swiss} is shown on Fig. 5 (1), with samples contained in a cell marked by the same color. According to Fig. 4 (right), points in μ_m are mainly located on the strip with only one point off in the most sparse cell (yellow cell located in the bottom in the figure).

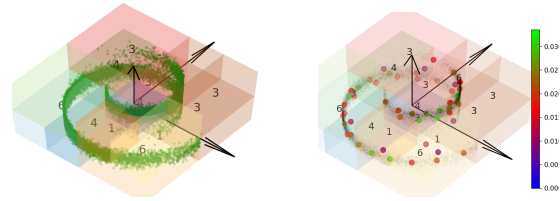


Figure 4. On Swiss Roll. Left: 15000 samples from the truncated normal mixture distribution μ_{swiss} over X_{swiss} ; Right: 50-point 3D discretization using Algorithm 2, the refinement cells are shown in colored boxes.

On the other hand, consider the metric on X_{swiss} induced by the isometry from the Swiss Roll as a manifold to a strip on \mathbb{R}^2 . A more intrinsic discretization of μ_{swiss} can be obtained by applying EDOT through a refinement on the coordinate space, the (2D) strip. The partition of S_{swiss} is shown on Fig. 5 (2), and resulting discretization μ_{50} is shown in Fig. 5 (3). Notice that all 50 points are located on the (locally) high density region of the Swiss Roll. We observe from Fig. 5 (1) and (2) that the 3D partition may pull disconnected and intrinsically remote regions together while the 2D partition maintains the intrinsic structure.

On Sphere. The underlying space X_{sphere} is the unit sphere in \mathbb{R}^3 . μ_{sphere} is the pushforward of a normal mixture distribution on \mathbb{R}^2 by stereographic projection. The sample set $S_{\text{sphere}} \sim \mu_{\text{sphere}}$ over X_{sphere} is shown on Fig. 6 left.

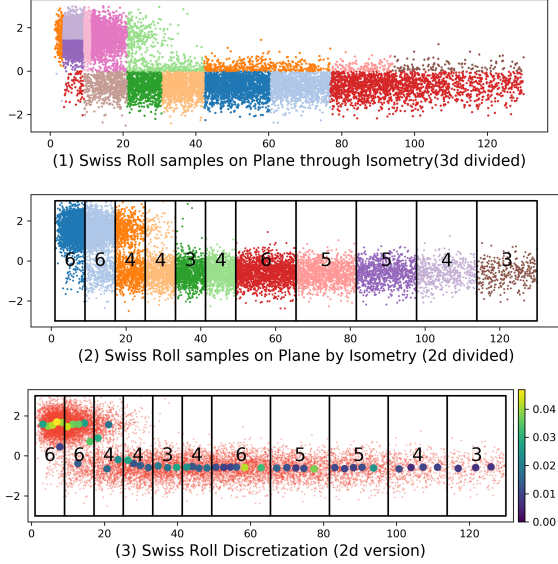


Figure 5. Swiss Roll under Isometry. (1) Refinement Cells under 3D Euclidean metric (one color per samples from a refinement cell); (2) Refinement Cells under 2D metric induced by the isometry; (3) EDOT of 50 points with respect to the 2D refinement.

Consider the (3D) Euclidean metric on X_{sphere} induced by the the embedding, Fig. 6 (right) plots the EDOT solution with refinement for μ_m with $m = 40$. The resulting cell structure is shown as colored boxes.

To consider the intrinsic metric, a CW-complex is constructed. The structure is built with a point on the equator as a 0-cell structure, the rest of the equator as a 1-cell, and the upper hemisphere and lower hemisphere as two dimension-2 (open) cells. We take the upper and lower hemispheres and map them onto unit disc through stereographic projection with respect to south pole and north pole, respectively. Then we take the metric from spherical geometry, and rewrite the distance function and its gradient using the natural coordinate on the unit disc (see Supplementary for details.) Fig. 7 shows the refinement of EDOT on the samples (in red) and corresponding discretizations in colored points. More figures can be found in the Supplementary.

5.3. An Example on Transference Plan with ACR

We now illustrate the performance of Adaptive EDOT on a 2D optimal transport task. Let $X = Y = [0, 1]^2$, $c = d_X$ be the Euclidean distance, $g = d_X^2$, and the marginal μ, ν be truncated normal (mixtures), where μ has only 2 components and ν has 5 components. Fig. 8 plots the McCann Interpolation of the OT plan of between μ and ν (shown in red dots) and its discrete approximations (weights are color coded) with $m = n = 30$. With $m = n = 10$, Adaptive EDOT results: $W_{k,\zeta}^k(\mu, \mu_{10}) = 1.33 \times 10^{-2}$,

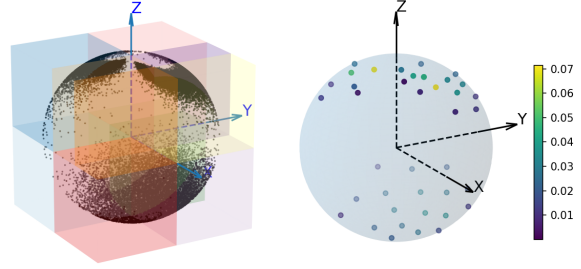


Figure 6. Left: 30000 samples on sphere; Right: EDOT of 40 points in 3D.

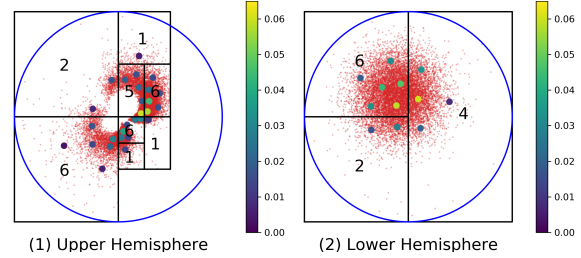


Figure 7. CW-EDOT of 40 points in 2D. Left: upper hemisphere; Right: lower hemisphere, by stereographic projections about poles.

$W_{k,\zeta}^k(\nu, \nu_{10}) = 1.30 \times 10^{-2}$, $W_{k,\zeta}^k(\gamma, \gamma_{10,10}) = 2.71 \times 10^{-2}$. With $m = n = 30$, Adaptive EDOT results, $W_{k,\zeta}^k(\mu, \mu_{30}) = 9.62 \times 10^{-3}$, $W_{k,\zeta}^k(\nu, \nu_{30}) = 9.18 \times 10^{-3}$, $W_{k,\zeta}^k(\gamma, \gamma_{30,30}) = 1.516 \times 10^{-2}$. Where as naive sampling results: $W_{k,\zeta}^k(\mu, \mu'_{30}) = 1.75 \times 10^{-2}$, $W_{k,\zeta}^k(\nu, \nu'_{30}) = 1.58 \times 10^{-2}$, $W_{k,\zeta}^k(\gamma, \gamma'_{30,30}) = 3.95 \times 10^{-2}$. Adaptive EDOT approximated the quality of 900 naive samples with only 100 points on a 4 dimensional transference plan.

6. Analysis of the Algorithms

6.1. On Algorithm 1

First, for each iteration in the minibatch SGD, let N be the sample (minibatch) size of μ_N for approximating μ . Let m be the size of target discretization μ_m (the output). Further let d be the dimension of X , ϵ be the error bound in Sinkhorn calculation for the entropy-regularized optimal transference plan between μ_N and μ_m . The Sinkhorn algorithm for the positive matrix $e^{-g(x,y)/\zeta}$ (of size $N \times m$) converges linearly, which takes $\mathcal{O}(\log(1/\epsilon))$ steps to fall into a region of radius ϵ , contributing $\mathcal{O}(Nm \log(1/\epsilon))$ in time complexity. The inverse matrix \mathbf{M} of $\nabla_{(\alpha,\beta)} \mathcal{N} = -\frac{1}{\zeta} \begin{bmatrix} A & B \\ B^T & D \end{bmatrix}$ (Eq. (8)) is taken block-wise (see Supplementary for details):

$$\mathbf{M} = -\zeta \begin{bmatrix} A^{-1} + A^{-1}BE^{-1}B^TA^{-1} & -A^{-1}BE^{-1} \\ -E^{-1}B^TA^{-1} & E^{-1} \end{bmatrix}$$

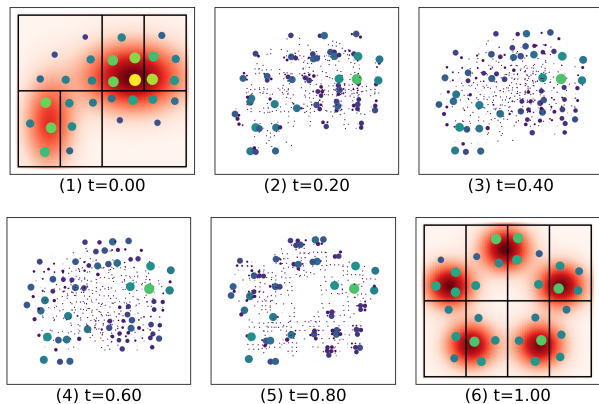


Figure 8. McCann Interpolation (See Supplementary for more slices and animation) of 30×30 transference plan.

where $E = D - B^T A^{-1} B$. Block E is constructed in $\mathcal{O}(Nm^2)$ and inverted in $\mathcal{O}(m^3)$; block $A^{-1} B E^{-1}$ takes $\mathcal{O}(Nm^2)$ as A is diagonal; and the block $A^{-1} + A^{-1} B E^{-1} B^T A^{-1}$ takes $\mathcal{O}(N^2 m)$ to construct. When $m \ll N$, the time complexity in constructing \mathbf{M} is $\mathcal{O}(N^2 m)$. From \mathbf{M} to gradient of dual variables: the tensor contractions have complexity $\mathcal{O}((N + m)^2 m d)$. Finally, to get the gradient, the complexity is dominated by the second term of Eq. (7), which is a contraction between a matrix Nm (i.e., $gd\pi(x)$) with tensors of sizes Nmd and $m^2 d$ (two gradients on dual variables α, β) along N and m respectively. Thus the final step contributes $\mathcal{O}((N + m)md)$.

The time complexity of increment steps in SGD turns out to be $\mathcal{O}(md)$. Therefore, for L steps of minibatch SGD, the time complexity is $\mathcal{O}((N + m)^2 mdL + NmL \log(1/\epsilon))$.

For space complexity, Sinkhorn algorithm (which can be done in position $\mathcal{O}(Nm)$) is the only iterative computation in a single SGD step, and between two SGD steps, only the resulting distribution is passed to next step. Therefore, the space complexity is $\mathcal{O}((N + m)^2)$ coming from the \mathbf{M} , others are at most of size $\mathcal{O}(m(N + m))$.

From the above discussion, we can further see that when Algorithm 2 is applied, the total complexities (both in time and space) are reduced as the magnitudes of both N and m are much smaller in each refined cell.

Finally, the convergence rate affects the time complexity. Since minibatch SGD is applied, the convergence rate depends on the choice of the initial distribution, and is also affected by the size m , N , and the diameter of the cell.

6.2. On Algorithm 2

The procedure of dividing sample set S into subsets in Algorithm 2 is similar to Quicksort, thus the space and time complexities are similar. The similarity comes from the bi-

nary divide-and-conquer structure as well as that each split action is based on comparing each sample with a target (the “mid” in Algorithm 2).

The time complexity of Algorithm 2 is $\mathcal{O}(N_0 \log N_0)$ in best and average case, $\mathcal{O}(N_0^2)$ in worst case (which would happen when each cell contains only one sample). The time complexity depends only on the distribution, not on the order the samples are stored.

The space complexity is $\mathcal{O}(N_0 d + m)$, or simply $\mathcal{O}(N_0 d)$ as $m \ll N_0$. Furthermore, if we use swap to make the split of sample size “in position” (as in Quicksort), we may only need space for one copy of set S (of size $N_0 d$), those in DFS stack and output stack (proportional to m) and some fixed size space for calculations.

The applications of Algorithm 1 on the cells are independent from each other, making the computation parallelizable. And the post-processing of such parallelization takes only m multiplications and a concatenation to construct μ_m .

6.3. Comparison with Naive Sampling

After having a size- m discretization on X and a size- n discretization on Y , the EOT solution (Sinkhorn algorithm) has time complexity $\mathcal{O}(mn \log(1/\epsilon))$. In EDOT, two discretization problems must be solved before applying Sinkhorn, while the naive sampling requires nothing but sampling.

According to the previous analysis, solving a single continuous EOT problem using size- m EDOT method directly may result in higher time complexity than naive sampling with even a larger sample size (than m), when the cost function $c : X \times Y \rightarrow \mathbb{R}$ is completely known. However, in real applications, the cost function may be from real world experiments (or from extra computations) done for each pair (x, y) in the discretization, thus the size of discretized distribution is critical for cost-control, but the distance function d_X and d_Y usually come along with the spaces X and Y and are easy to calculate. Another scenario of application of EDOT is that the marginal distributions μ_X and ν_Y are fixed for different cost functions, then discretizations can be reused, thus the cost of discretization is one-time and improvement it brings accumulates in each repeat.

7. Conclusion

We developed methods for efficiently approximating OT couplings with fixed size $m \times n$ approximations. We provided bounds on the relationship between the discrete approximation and the original continuous problem. We implemented two algorithms and demonstrated their efficacy as compared to naive sampling and analyzed computational complexity. Our approach provides a new approach to efficiently computing OT plans.

A. Proof of Proposition 2.1

Proposition 2.1. *When X and Y are two compact spaces and c is C^∞ , there exists a constant $C_1 \in \mathbb{R}^+$ such that*

$$\begin{aligned} \max\{W_k^k(\mu, \mu_m), W_k^k(\nu, \nu_n)\} &\stackrel{(i)}{\leq} W_{k,\zeta}^k(\gamma_\lambda(\mu, \nu), \gamma_\lambda(\mu_m, \nu_n)) \\ &\stackrel{(ii)}{\leq} C_1[W_{k,\zeta}^k(\mu, \mu_m) + W_{k,\zeta}^k(\nu, \nu_n)]. \end{aligned} \quad (11)$$

Proof. We will adopt notations: $Z = X \times Y$ and $z_i = (x_i, y_i) \in Z$.

For inequality (i), without loss assume that

$$\max\{W_k^k(\mu, \mu_m), W_k^k(\nu, \nu_n)\} = W_k^k(\mu, \mu_m)$$

Denote the optimal $\pi_Z \in \Pi(\gamma_\lambda(\mu, \nu), \gamma_\lambda(\mu_m, \nu_n))$ that achieves $W_k^k(\gamma_\lambda(\mu, \nu), \gamma_\lambda(\mu_m, \nu_n))$ by π_Z^* similarly for π_X^* . Then we have:

$$\begin{aligned} W_k^k(\gamma_\lambda(\mu, \nu), \gamma_\lambda(\mu_m, \nu_n)) &= \int_{Z^2} d_Z^k(z_1, z_2) d\pi_Z^* \geq A \int_{Z^2} d_X^k(x_1, x_2) d\pi_Z^* \\ &= A \int_{X^2} d_X^k(x_1, x_2) \int_{Y^2} d\pi_Z^* \stackrel{(a)}{=} A \int_{X^2} d_X^k(x_1, x_2) d\pi_X^* \\ &\stackrel{(b)}{\geq} A \int_{X^2} d_X^k(x_1, x_2) d\pi_X^* = W_k^k(\mu, \mu_m) \end{aligned}$$

Here $\pi_X^* \in \Pi(\mu, \mu_m)$, eq (a) holds since $\pi_Z^* \in \Pi(\gamma_\lambda(\mu, \nu), \gamma_\lambda(\mu_m, \nu_n))$ and ineq (b) holds since π_X^* is the optimal choice.

For inequality (ii), we will use the following to simplify the notations,

$$d\gamma \otimes d\gamma_{mn} := d\gamma_\lambda(\mu, \nu) \otimes d\gamma_\lambda(\mu_m, \nu_n)$$

$$d_Z^k := d_Z^k(z_1, z_2), d_X^k := d_X^k(x_1, x_2), d_Y^k := d_Y^k(y_1, y_2)$$

$$\begin{aligned} W_{k,\zeta}^k(\gamma_\lambda(\mu, \nu), \gamma_\lambda(\mu_m, \nu_n)) &= \int_{Z^2} d_Z^k(z_1, z_2) d\pi_{z,\zeta}^* \\ &\stackrel{(a)}{=} \int_{Z^2} d_Z^k \cdot \exp\left(\frac{\alpha(z_1) + \beta(z_2) - d_Z^k(z_1, z_2)}{\zeta}\right) d\gamma \otimes d\gamma_{mn} \\ &\stackrel{(b)}{\leq} A \int_{Z^2} (d_X^k + d_Y^k) \cdot \exp\left(\frac{\alpha(z_1) + \beta(z_2) - d_Z^k(z_1, z_2)}{\zeta}\right) d\gamma \otimes d\gamma_{mn} \\ &\stackrel{(c)}{\leq} C_1 \int_{Z^2} (d_X^k + d_Y^k) \cdot \exp\left(\frac{-d_Z^k}{\zeta}\right) d\gamma \otimes d\gamma_{mn} \\ &\stackrel{(d)}{\leq} C_1 \left[\int_{Z^2} d_X^k \cdot \exp\left(\frac{-d_X^k}{\zeta}\right) + d_Y^k \cdot \exp\left(\frac{-d_Y^k}{\zeta}\right) d\gamma \otimes d\gamma_{mn} \right] \\ &\stackrel{(e)}{=} C_1 \left[\int_{X^2} d_X^k \cdot \exp\left(\frac{-d_X^k}{\zeta}\right) d\mu \otimes d\mu_m \right. \\ &\quad \left. + \int_{Y^2} d_Y^k \cdot \exp\left(\frac{-d_Y^k}{\zeta}\right) d\nu \otimes d\nu_n \right] \\ &\stackrel{(f)}{\leq} C_1 \int_{X^2} d_X^k \cdot \exp\left(\frac{s(x_1) + t(x_2) - d_X^k}{\zeta}\right) d\mu \otimes d\mu_m \\ &\quad + C_1 \int_{Y^2} d_Y^k \cdot \exp\left(\frac{s'(y_1) + t'(y_2) - d_Y^k}{\zeta}\right) d\nu \otimes d\nu_n \\ &= C_1 [W_{k,\zeta}^k(\mu, \mu_m) + W_{k,\zeta}^k(\nu, \nu_n)] \end{aligned}$$

Justifications for the derivations:

(a) Based on the dual formulation, it is shown in (Aude et al., 2016)[Proposition 2.1] that for $\zeta > 0$, there exist $\alpha(z_1), \beta(z_2) \in \mathcal{C}(Z)$ such that $d\pi_{z,\zeta}^* = \exp\left(\frac{\alpha(z_1) + \beta(z_2) - d_Z^k(z_1, z_2)}{\zeta}\right) d\gamma \otimes d\gamma_{mn}$;

(b) Inequality (ii) of eq (3);

(c) According to (Genevay et al., 2019)[Theorem 2], when X, Y are compact and c is smooth, α, β are uniformly bounded; moreover both d_X^k and d_Y^k are uniformly bounded by the diameter of X and Y respectively, hence constant B exists;

(d) Inequality (ii) of eq (3);

(e) $\gamma_\lambda(\mu, \nu) \in \Pi(\mu, \nu)$ and $\gamma_\lambda(\mu_m, \nu_n) \in \Pi(\mu_m, \nu_n)$;

(f) Similarly as in (a), for $\zeta > 0$, there exist $s(x_1), t(x_2) \in \mathcal{C}(X)$ and $s'(y_1), t'(y_2) \in \mathcal{C}(Y)$ such that $\exp\left(\frac{-d_X^k}{\zeta}\right) d\mu \otimes d\mu_m = d\pi_X^*$ and $\exp\left(\frac{-d_Y^k}{\zeta}\right) d\nu \otimes d\nu_n = d\pi_Y^*$. Moreover, $\int_{X^2} d_X^k \cdot \exp\left(\frac{s(x_1) + t(x_2) - d_X^k}{\zeta}\right) d\mu \otimes d\mu_m \geq 0$ and $\int_{Y^2} d_Y^k \cdot \exp\left(\frac{s'(y_1) + t'(y_2) - d_Y^k}{\zeta}\right) d\nu \otimes d\nu_n \geq 0$. \square

B. Gradient of $W_{k,\zeta}^k$

B.1. The Gradient

Following the definitions and notations in Section 2 and Section 3 of the paper, we calculate the gradient of $W_{k,\zeta}^k(\mu, \mu_m)$ about parameters of $\mu_m := \sum_{i=1}^m w_i \delta_{y_i}$ in detail.

$W_{k,\zeta}^k(\mu, \mu_m) = \int_{X^2} g(x, y) d\gamma_\zeta(x, y)$ where

$$\gamma_\zeta = \operatorname{argmin}_{\gamma \in \Pi(\mu, \mu_m)} \int_{X^2} g(x, y) d\gamma(x, y) + \zeta \operatorname{KL}(\gamma \| \mu \otimes \mu_m). \quad (12)$$

Let $\alpha \in L^\infty(X)$ and $\beta \in \mathbb{R}^m$, denote $\beta = \sum_{i=1}^m \beta_i \delta_{y_i}$, let

$$\begin{aligned} & \mathcal{F}(\gamma; \mu, \mu_m, \alpha, \beta) \\ &:= \int_{X^2} g(x, y) d\gamma(x, y) + \zeta \operatorname{KL}(\gamma \| \mu \otimes \mu_m) \\ & \quad + \int_X \alpha(x) \left(\int_X d\gamma(x, y) - d\mu_m(y) \right) \\ & \quad + \int_X \beta(y) \left(\int_X d\gamma(x, y) - d\mu(x) \right) \\ &= \int_{X^2} g(x, y) d\gamma(x, y) + \zeta \operatorname{KL}(\gamma \| \mu \otimes \mu_m) \\ & \quad + \int_X \alpha(x) \left(\sum_{i=1}^m d\gamma(x, y_i) - d\mu_m(y_i) \right) \\ & \quad + \sum_{i=1}^m \beta_i \left(\int_X d\gamma(x, y_i) - d\mu(x) \right) \end{aligned} \quad (13)$$

Since γ on second component X is discrete and supported on $\{y_i\}_{i=1}^m$, we may denote $d\gamma(x, y_i)$ by $d\pi_i(x)$, thus

$$\begin{aligned} & \mathcal{F}(\gamma; \mu, \mu_m, \alpha, \beta) \\ &= \int_X \sum_{i=1}^m g(x, y_i) d\pi_i(x) \\ & \quad + \zeta \sum_{i=1}^m \int_X \left(\ln \frac{d\pi_i(x)}{d\mu(x)} - \ln(\mu_m(y_i)) \right) d\pi_i(x) \\ & \quad + \int_X \alpha(x) \left(\sum_{i=1}^m d\pi_i(x) - d\mu_m(y_i) \right) \\ & \quad + \sum_{i=1}^m \beta_i \left(\int_X d\pi_i(x) - d\mu(x) \right) \end{aligned} \quad (14)$$

Then the Fenchel duality of Problem (12) is

$$\begin{aligned} & \mathcal{L}(\mu, \mu_m; \alpha, \beta) \\ &= \int_X \alpha(x) d\mu(x) + \sum_{i=1}^m \beta_i w_i \\ & \quad - \zeta \int_X \sum_{i=1}^m e^{(\alpha(x) + \beta_i - g(x, y_i)) / \zeta} w_i d\mu(x). \end{aligned} \quad (15)$$

Let α^*, β^* be the argmax of the Fenchel dual (15), the primal is solved by $d\gamma^*(x, y_i) = e^{(\alpha^*(x) + \beta_i^* - g(x, y_i)) / \zeta} w_i d\mu(x)$. To make the solution unique, we restrict the freedom of solution (where we see that $\mathcal{L}(\mu, \mu_m; \alpha, \beta) = \mathcal{L}(\mu, \mu_m; \alpha + t, \beta - t)$ for any $t \in \mathbb{R}$). We use the condition $\beta_m = 0$ to narrow the choices down to only one, and denote the dual variable β having the property by $\bar{\beta}$ and $\bar{\beta}^*$.

We first calculate $\nabla_{w_i, y_i} \mathcal{L}(\mu, \mu_m; \alpha^*, \bar{\beta}^*)$ with α^* and $\bar{\beta}^*$ as functions of μ_m . (From the paper)

$$\begin{aligned} & \frac{\partial \mathcal{L}}{\partial w_i} = \int_X g(x, y_i) E_i^*(x) d\mu(x) + \\ & \quad \frac{1}{\zeta} \int_X \sum_{j=1}^n g(x, y_j) \left(\frac{\partial \alpha^*(x)}{\partial w_i} + \frac{\partial \beta_j^*}{\partial w_i} \right) w_j E_j^*(x) d\mu(x). \end{aligned} \quad (16)$$

$$\begin{aligned} & \nabla_{y_i} \mathcal{L} = \int_X \nabla_{y_i} g(x, y_i) \left(1 - \frac{g(x, y_i)}{\zeta} \right) E_i^*(x) w_i d\mu(x) + \\ & \quad \frac{1}{\zeta} \int_X \sum_{j=1}^n g(x, y_j) (\nabla_{y_i} \alpha^*(x) + \nabla_{y_i} \beta_j^*) w_j E_j^*(x) d\mu(x). \end{aligned} \quad (17)$$

Next, we calculate the derivatives of α^* and $\bar{\beta}^*$, by finding their defining equation and then using Implicit Function Theorem.

The optimal solution to the dual variables α^*, β^* is obtained by solving the stationary state equation $\nabla_{\alpha, \beta} \mathcal{L} = 0$. The derivatives are taken in the sense of Fréchet derivative. The Fenchel dual function on $\alpha, \bar{\beta}$, has its domain and codomain $\mathcal{L}(\mu, \mu_m; \cdot, \cdot) : L^\infty(X) \times \mathbb{R}^{m-1} \rightarrow \mathbb{R}$, the derivatives are

$$\begin{aligned} & \nabla_\alpha \mathcal{L}(\mu, \mu_m; \alpha, \bar{\beta}) \\ &= \int_X \left(1 - \sum_{i=1}^m w_i E_i(x) \right) (\cdot) d\mu(x), \end{aligned} \quad (18)$$

$$\frac{\partial}{\partial \beta_i} \mathcal{L}(\mu, \mu_m; \alpha, \bar{\beta}) = w_i \left(1 - \int_X E_i(x) d\mu(x) \right) \quad (19)$$

where $E_i(x) = e^{(\alpha(x) + \beta_i - g(x, y_i)) / \zeta}$ is defined as in the paper, and $\nabla_\alpha \mathcal{L}(\mu, \mu_m; \alpha, \bar{\beta}) \in (L^\infty(X))^\vee$ (as a linear functional), $\frac{\partial}{\partial \beta_i} \mathcal{L}(\mu, \mu_m; \alpha, \bar{\beta}) \in \mathbb{R}$. Next, we need to show \mathcal{L} is differentiable in the sense of Fréchet derivative, i.e.,

$$\begin{aligned} & \lim_{\|h\| \rightarrow 0} \frac{1}{\|h\|} \left(\mathcal{L}(\mu, \mu_m; \alpha + h, \bar{\beta}) - \mathcal{L}(\mu, \mu_m; \alpha, \bar{\beta}) \right. \\ & \quad \left. - \nabla_\alpha \mathcal{L}(\mu, \mu_m; \alpha, \bar{\beta})(h) \right) = 0. \end{aligned} \quad (20)$$

By definition of \mathcal{L} (we write $\mathcal{L}(\alpha)$ for $\mathcal{L}(\mu, \mu_m; \alpha, \bar{\beta})$),

$$\begin{aligned}
 & \mathcal{L}(\alpha + h) - \mathcal{L}(\alpha) - \nabla_{\alpha} \mathcal{L}(\alpha)(h) \\
 &= \int_X h(x) d\mu(x) - \zeta \int_X \sum_{i=1}^m \left(e^{h(x)/\zeta} - 1 \right) w_i E_i(x) d\mu(x) \\
 & \quad - \int_X \left(1 - \sum_{i=1}^m w_i E_i(x) \right) h(x) d\mu(x) \\
 &= \zeta \int_X \sum_{i=1}^m \left(1 + \frac{h(x)}{\zeta} - e^{h(x)/\zeta} \right) E_i(x) w_i d\mu(x) \\
 &= \zeta \int_X \left(\sum_{k=2}^{\infty} \frac{1}{k!} \frac{h(x)^k}{\zeta^k} \right) \sum_{i=1}^m E_i(x) w_i d\mu(x), \quad (21)
 \end{aligned}$$

the last equality is from the Taylor expansion of exponential function. Consider that $\|h\|_{\infty} = \text{ess sup}_{x \in X} |h(x)|$ the essential supremum of $|h(x)|$ for $x \in X$ given measure μ .

Denote $\mathcal{N} := \nabla_{\alpha, \bar{\beta}} \mathcal{L}$,

$$\begin{aligned}
 & \frac{1}{\|h\|} (\mathcal{L}(\alpha + h) - \mathcal{L}(\alpha) - \nabla_{\alpha} \mathcal{L}(\alpha)(h)) \\
 & \leq \frac{\zeta}{\|h\|} \int_X \left(\sum_{k=2}^{\infty} \frac{1}{k!} \frac{|h(x)|^k}{\zeta^k} \right) \sum_{i=1}^m E_i(x) w_i d\mu(x) \\
 & \leq \frac{\zeta}{\|h\|} \int_X \left(\sum_{k=2}^{\infty} \frac{1}{k!} \frac{\|h\|^k}{\zeta^k} \right) \sum_{i=1}^m E_i(x) w_i d\mu(x) \\
 & = \zeta \left(\sum_{k=2}^{\infty} \frac{1}{k!} \frac{\|h\|^{k-1}}{\zeta^k} \right) \int_X \sum_{i=1}^m E_i(x) w_i d\mu(x) \\
 & = \zeta \left(\sum_{k=2}^{\infty} \frac{1}{k!} \frac{\|h\|^{k-1}}{\zeta^k} \right) \quad (22)
 \end{aligned}$$

Therefore,

$$\lim_{\|h\| \rightarrow 0} \frac{1}{\|h\|} (\mathcal{L}(\alpha + h) - \mathcal{L}(\alpha) - \nabla_{\alpha} \mathcal{L}(\alpha)(h)) = 0, \quad (23)$$

which shows that the expression of $\nabla_{\alpha} \mathcal{L}(\alpha)$ in Eq. (18) gives the correct Fréchet derivative. Note here that $\alpha \in L^{\infty}(X)$ is critical in Eq. (22).

Let $\mathcal{N} := \nabla_{\alpha, \bar{\beta}} \mathcal{L}$ values in $(L^{\infty}(X))^{\vee} \times \mathbb{R}^{m-1}$, then $\mathcal{N} = 0$ defines α^* and $\bar{\beta}^*$, which makes it possible to differentiate them about μ_m using Implicit Function Theorem for Banach spaces. From now on, \mathcal{N} take values at $\alpha = \alpha^*$, $\bar{\beta} = \bar{\beta}^*$, i.e., the marginal conditions on $d\pi_i(x) = w_i E_i(x) d\mu(x)$ hold.

Thus we need $\nabla_{\alpha, \bar{\beta}} \mathcal{N}$ and $\nabla_{w_i, y_i} \mathcal{N}$ calculated, and prove that $\nabla_{\alpha, \bar{\beta}} \mathcal{N}$ is invertible (and give the inverse).

It is necessary to make sure which form $\nabla_{\alpha, \bar{\beta}} \mathcal{N}$ is in according to Fréchet derivative. Start from the map $\mathcal{N}(\mu, \mu_m; \cdot, \cdot) : (L^{\infty}(X)) \times \mathbb{R}^{m-1} \rightarrow (L^{\infty}(X))^{\vee} \times$

$(\mathbb{R}^{m-1})^{\vee}$ where \mathbb{R}^{m-1} is isomorphic to its dual Banach space $(\mathbb{R}^{m-1})^{\vee}$. Then $\nabla_{\alpha, \bar{\beta}} \mathcal{N} \in \text{Hom}_{\mathbb{R}}^b(L^{\infty}(X) \times \mathbb{R}^{m-1}, (L^{\infty}(X))^{\vee} \times (\mathbb{R}^{m-1})^{\vee})$, where Hom^b represents the set of bounded linear operators. Moreover, recall that $(\cdot) \otimes A$ is the left adjoint functor of $\text{Hom}_{\mathbb{R}}^b(A, \cdot)$, then for \mathbb{R} -vector spaces, $\text{Hom}_{\mathbb{R}}^b(L^{\infty}(X) \times \mathbb{R}^{m-1}, (L^{\infty}(X))^{\vee} \times (\mathbb{R}^{m-1})^{\vee}) \cong \text{Hom}_{\mathbb{R}}^b((L^{\infty}(X) \times \mathbb{R}^{m-1})^{\otimes 2}, \mathbb{R})$. Thus, we can write $\nabla_{\alpha, \bar{\beta}} \mathcal{N}$ in terms of a bilinear form on vector space $L^{\infty}(X) \times \mathbb{R}^{m-1}$.

From the expression of \mathcal{N} , we may differentiate (similarly as the calculations (21) to (23)):

$$\begin{aligned}
 \nabla_{\alpha} \mathcal{N} &= \left(-\frac{1}{\zeta} \int_X (\cdot)(-) \sum_{i=1}^m w_i E_i(x) d\mu(x), \right. \\
 & \quad \left. -\frac{1}{\zeta} \int_X (\cdot) w_i E_i(x) d\mu(x) \right) \quad (24)
 \end{aligned}$$

$$\begin{aligned}
 \nabla_{\bar{\beta}} \mathcal{N} &= \left(-\frac{1}{\zeta} \int_X (\cdot) w_i E_i(x) d\mu(x), \right. \\
 & \quad \left. -\frac{\delta_{ij}}{\zeta} \int_X w_i E_i(x) d\mu(x) \right) \quad (25)
 \end{aligned}$$

Consider the boundary conditions: $\sum_{i=1}^m w_i E_i(x) d\mu(x) = \sum_{i=1}^m d\pi_i(x) = \mu(x)$ and $\int_X w_i E_i(x) d\mu(x) = \int_X \pi_i(x) = w_i$, the $\nabla_{\alpha, \bar{\beta}} \mathcal{N}$ as the Hessian form of \mathcal{L} , can be written as

$$\nabla_{\alpha, \bar{\beta}} \mathcal{N} = -\frac{1}{\zeta} \begin{bmatrix} \langle \cdot, \cdot \rangle & \langle \pi_j, \cdot \rangle \\ \langle \cdot, \pi_i \rangle & w_i \delta_{ij} \end{bmatrix} \quad (26)$$

with $\langle \phi_1, \phi_2 \rangle = \int_X \phi_1(x) \phi_2(x) \mu(x)$, or further

$$\nabla_{\alpha, \bar{\beta}} \mathcal{N} = -\frac{1}{\zeta} \begin{bmatrix} d\mu(x) d\mu(x') \delta(x, x') & d\pi_j(x) \\ d\pi_i(x') & w_i \delta_{ij} \end{bmatrix} \quad (27)$$

over the basis $\{\delta(x), \mathbf{e}_i\}_{x \in X, i < m}$.

By the inverse of $\nabla_{\alpha, \bar{\beta}} \mathcal{N}$ we mean the element in $\text{Hom}_{\mathbb{R}}^b((L^{\infty}(X))^{\vee} \times (\mathbb{R}^{m-1})^{\vee}, L^{\infty}(X) \times \mathbb{R}^{m-1})$ which compose with $\nabla_{\alpha, \bar{\beta}} \mathcal{N}$ (on left and on right) are identities. By the natural identity between double dual $V^{\vee\vee} \cong V$ and the Tensor-Hom adjunction,

$$\begin{aligned}
 & \text{Hom}_{\mathbb{R}}^b((L^{\infty}(X))^{\vee} \times (\mathbb{R}^{m-1})^{\vee}, L^{\infty}(X) \times \mathbb{R}^{m-1}) \\
 & \cong \text{Hom}_{\mathbb{R}}^b((L^{\infty}(X))^{\vee} \times (\mathbb{R}^{m-1})^{\vee}, (L^{\infty}(X) \times \mathbb{R}^{m-1})^{\vee\vee}) \\
 & \cong \text{Hom}_{\mathbb{R}}^b(((L^{\infty}(X))^{\vee} \times (\mathbb{R}^{m-1})^{\vee})^{\otimes 2}, \mathbb{R}), \quad (28)
 \end{aligned}$$

we can write the inverse of $\nabla_{\alpha, \bar{\beta}} \mathcal{N}$ as a bilinear form again.

Denote $\nabla_{\alpha, \bar{\beta}} \mathcal{N}$ in the block form $\begin{bmatrix} A & B \\ B^T & D \end{bmatrix}$. According

to the block-inverse formula

$$\begin{bmatrix} A & B \\ B^T & D \end{bmatrix}^{-1} = \begin{bmatrix} A^{-1} + A^{-1} B F^{-1} B^T A^{-1} & -A^{-1} B F^{-1} \\ -F^{-1} B^T A^{-1} & F^{-1} \end{bmatrix} \quad (29)$$

where $F = D - B^T A^{-1} B$ whose invertibility determines the invertibility of $\begin{bmatrix} A & B \\ B^T & D \end{bmatrix}$.

Consider that $A^{-1} \in \text{Hom}_{\mathbb{R}}^b((L^\infty(X)^\vee)^{\otimes 2}, \mathbb{R})$, explicitly, $A^{-1}(x, y) = \delta(x, y)$. Therefore, from Eq. (27),

$$\begin{aligned} F_{ij} &= \delta_{ij} w_i - \int_{X^2} \delta(x, x') \pi_i(x) \pi_j(x') \\ &= \delta_{ij} w_i - \int_X w_i w_j E_i(x) E_j(x) \mu(x). \end{aligned} \quad (30)$$

The matrix F is symmetric, of rank $m - 1$ and strictly diagonally dominant, therefore it is invertible. To see the strictly diagonal dominance, consider $\sum_{j=1}^m \int_X w_i w_j E_i(x) E_j(x) \mu(x) = \int_X w_i E_i(x) \sum_{j=1}^m w_j E_j(x) \mu(x) = \int_X w_i E_i(x) \mu(x) = w_i$ by applying the marginal conditions, and that the matrix F is of size $(m - 1) \times (m - 1)$ (there is no $i = m$ or $j = m$ for F_{ij}), then the matrix F is strictly diagonally dominant.

With all ingredients known in formula (29), we can calculate the inverse of $\nabla_{\alpha, \bar{\beta}} \mathcal{N}$.

Following the implicit function theorem, we need $\nabla_{w_i, y_i} \mathcal{N}$, each partial derivative is an element in $L^\infty(X)^\vee \times \mathbb{R}^{m-1}$.

$$\begin{aligned} \frac{\partial \mathcal{N}}{\partial w_i} &= \left(- \int_X E_i(x) (\cdot) d\mu(x), \delta_{ij} \left(1 - \int_X E_i(x) d\mu(x) \right) \right) \\ &= \left(- \int_X (\cdot) E_i(x) d\mu(x), 0 \right). \end{aligned} \quad (31)$$

Note that if we apply the constraint $\sum_{i=1}^m w_i = 1$ to w_i 's, we may set $w_m = 1 - \sum_{i=1}^{m-1} w_i$ and recalculate the above derivatives as $\nabla_{w_i} \mathcal{N} = \nabla_{w_i} \mathcal{N} - \nabla_{w_m} \mathcal{N}$ when $i \neq m$, and $\nabla_{w_m} \mathcal{N} = \sum_{i=1}^{m-1} \nabla_{w_i} \mathcal{N}$.

$$\begin{aligned} \nabla_{y_i} \mathcal{N} &= \left(\frac{1}{\zeta} \int_X (\cdot) \nabla_{y_i} g(x, y_i) w_i E_i(x) d\mu(x) \right. \\ &\quad \left. \frac{\delta_{ij}}{\zeta} \int_X \nabla_{y_i} g(x, y_i) w_i E_i(x) d\mu(x) \right) \end{aligned} \quad (32)$$

Finally, by implicit function theorem, $\nabla_{w_i, y_j} (\alpha^*, \bar{\beta}^*) = - \left(\nabla_{\alpha, \bar{\beta}} \mathcal{N} |_{\alpha^*, \bar{\beta}^*} \right)^{-1} \left(\nabla_{w_i, y_j} \mathcal{N} |_{\alpha^*, \bar{\beta}^*} \right)$ which fits in (16) and (17).

B.2. Second Derivatives

In this part, we calculate the second derivatives of $W_{k, \zeta}^k(\mu, \mu_m)$ with respect to the ingredients of μ_m , i.e., w_i 's and y_i 's, for the potential of applying Newton's method in EDOT (while we have not implemented yet).

Using the previous results, we can further calculate the second derivatives of $W_{k, \zeta}^k$ about w_i 's and y_i 's. Differentiating (16) and (17) results in

$$\begin{aligned} \frac{\partial^2 \mathcal{L}}{\partial w_i \partial w_j} &= \frac{1}{\zeta} \int_X g(x, y_j) \sum_{k=i, j} \left(\frac{\partial \alpha(x)}{\partial w_k} + \frac{\partial \bar{\beta}_k}{\partial w_k} \right) E_k(x) d\mu(x) \\ &\quad + \frac{1}{\zeta} \int_X \sum_{k=1}^n \left(\frac{\partial^2 \alpha(x)}{\partial w_i \partial w_j} + \frac{\partial^2 \bar{\beta}_k}{\partial w_i \partial w_j} \right) w_k E_k(x) d\mu(x) \\ &\quad + \frac{1}{\zeta^2} \int_X \sum_{k=1}^m \prod_{l=i, j} \left(\frac{\partial \alpha(x)}{\partial w_l} + \frac{\partial \bar{\beta}_k}{\partial w_l} \right) w_k E_k(x) d\mu(x) \end{aligned} \quad (33)$$

$$\begin{aligned} \nabla_{y_j} \frac{\partial \mathcal{L}}{\partial w_i} &= \delta_{ij} \left[\int_X \left(1 - \frac{g(x, y_i)}{\zeta} \right) \nabla_{y_i} E_i(x) d\mu(x) \right] \\ &\quad + \frac{1}{\zeta} \int_X \nabla_{y_j} g(x, y_j) \left(\frac{\partial \alpha(x)}{\partial w_i} + \frac{\partial \bar{\beta}_j}{\partial w_i} \right) w_j E_j(x) d\mu(x) \\ &\quad + \frac{1}{\zeta} \int_X g(x, y_j) \nabla_{y_j} \left(\frac{\partial \alpha(x)}{\partial w_i} + \frac{\partial \bar{\beta}_j}{\partial w_i} \right) w_j E_j(x) d\mu(x) \\ &\quad + \frac{1}{\zeta^2} \int_X \sum_{k=1}^m g(x, y_k) \left(\frac{\partial \alpha(x)}{\partial w_i} + \frac{\partial \bar{\beta}_k}{\partial w_i} \right) \\ &\quad \left(\nabla_{y_j} \alpha(x) + \nabla_{y_j} \bar{\beta}_k \right) w_k E_k(x) d\mu(x) \end{aligned} \quad (34)$$

$$\begin{aligned}
 & \nabla_{y_j} \nabla_{y_i} \mathcal{L} \\
 = & \delta_{ij} \left[\int_X \nabla_{y_i}^2 g(x, y_i) \left(1 - \frac{g(x, y_i)}{\zeta}\right) w_i E_i(x) d\mu(x) \right. \\
 & \left. - \frac{1}{\zeta} \int_X (\nabla_{y_i} g(x, y_i))^2 \left(2 - \frac{g(x, y_i)}{\zeta}\right) w_i E_i(x) d\mu(x) \right] \\
 & + \frac{1}{\zeta} \int_X \left(1 - \frac{g(x, y_i)}{\zeta}\right) \nabla_{y_i} g(x, y_i) \cdot \\
 & \quad (\nabla_{y_j} \alpha(x) + \nabla_{y_j} \bar{\beta}_i) w_i E_i(x) d\mu(x) \\
 & + \frac{1}{\zeta} \int_X \left(1 - \frac{g(x, y_j)}{\zeta}\right) \nabla_{y_j} g(x, y_j) \cdot \\
 & \quad (\nabla_{y_i} \alpha(x) + \nabla_{y_i} \bar{\beta}_j) w_j E_j(x) d\mu(x) \\
 & + \frac{1}{\zeta} \int_X \sum_{k=1}^m g(x, y_k) (\nabla_{y_i} \nabla_{y_j} \alpha(x) + \nabla_{y_i} \nabla_{y_j} \bar{\beta}_k) \cdot \\
 & \quad w_k E_k(x) d\mu(x) \\
 & + \frac{1}{\zeta^2} \int_X \sum_{k=1}^m g(x, y_k) \prod_{l=i,j} (\nabla_l \alpha + \nabla_l \bar{\beta}_k) \cdot \\
 & \quad w_k E_k(x) d\mu(x) \tag{35}
 \end{aligned}$$

Once we have the second derivatives of $g(x, y)$ on y_i 's, we need the second derivatives of α^* and $\bar{\beta}^*$ to build the above second derivatives. From the formula $\nabla_{w_i, y_j} (\alpha^*, \bar{\beta}^*) = -(\nabla_{\alpha, \bar{\beta}} \mathcal{N}|_{\alpha^*, \bar{\beta}^*})^{-1} (\nabla_{w_i, y_j} \mathcal{N}|_{\alpha^*, \bar{\beta}^*})$, we can differentiate

$$\begin{aligned}
 & \nabla_{w_k, y_l} \nabla_{w_i, y_j} (\alpha^*, \bar{\beta}^*) \\
 = & -\nabla_{w_k, y_l} \left(\nabla_{\alpha, \bar{\beta}} \mathcal{N}|_{\alpha^*, \bar{\beta}^*} \right)^{-1} \left(\nabla_{w_i, y_j} \mathcal{N}|_{\alpha^*, \bar{\beta}^*} \right) \\
 & - \left(\nabla_{\alpha, \bar{\beta}} \mathcal{N}|_{\alpha^*, \bar{\beta}^*} \right)^{-1} \left(\nabla_{w_k, y_l} \nabla_{w_i, y_j} \mathcal{N}|_{\alpha^*, \bar{\beta}^*} \right). \tag{36}
 \end{aligned}$$

Here from the formula that $\nabla A^{-1} = -A^{-1} \nabla A A^{-1}$ (this is the product rule for $AA^{-1} = I$), we have

$$\begin{aligned}
 & \nabla_{w_k, y_l} \left(\nabla_{\alpha, \bar{\beta}} \mathcal{N}|_{\alpha^*, \bar{\beta}^*} \right)^{-1} \\
 = & - \left(\nabla_{\alpha, \bar{\beta}} \mathcal{N}|_{\alpha^*, \bar{\beta}^*} \right)^{-1} \nabla_{w_k, y_l} \left(\nabla_{\alpha, \bar{\beta}} \mathcal{N}|_{\alpha^*, \bar{\beta}^*} \right) \\
 & \left(\nabla_{\alpha, \bar{\beta}} \mathcal{N}|_{\alpha^*, \bar{\beta}^*} \right)^{-1} \tag{37}
 \end{aligned}$$

and

$$\begin{aligned}
 & \nabla_{w_k} \left(\nabla_{\alpha, \bar{\beta}} \mathcal{N}|_{\alpha^*, \bar{\beta}^*} \right) \\
 = & -\frac{1}{\zeta} \begin{bmatrix} 0 & \delta_{jk} E_k(x) d\mu(x) \\ \delta_{ik} E_k(x') d\mu(x') & \delta_{ij} \delta_{jk} \end{bmatrix} \tag{38}
 \end{aligned}$$

$$\begin{aligned}
 & \nabla_{y_k} \left(\nabla_{\alpha, \bar{\beta}} \mathcal{N}|_{\alpha^*, \bar{\beta}^*} \right) \\
 = & \frac{1}{\zeta^2} \begin{bmatrix} 0 & \delta_{jk} \nabla_{y_k} g(x, y_k) d\pi_k(x) \\ \delta_{ik} \nabla_{y_k} g(x', y_k) d\pi_k(x') & 0 \end{bmatrix}. \tag{39}
 \end{aligned}$$

The last piece we need is $(\nabla_{w_k, y_l} \nabla_{w_i, y_j} \mathcal{N}|_{\alpha^*, \bar{\beta}^*})$:

$$\frac{\partial^2 \mathcal{N}}{\partial w_j \partial w_i} = (0, 0), \tag{40}$$

$$\begin{aligned}
 & \nabla_{y_j} \frac{\partial \mathcal{N}}{\partial w_i} \\
 = & \left(\frac{1}{\zeta} \int_X (\cdot) \nabla_{y_j} g(x, y_j) E_i(x) d\mu(x), 0 \right), \tag{41}
 \end{aligned}$$

$$\begin{aligned}
 & \nabla_{y_j} \nabla_{y_i} \mathcal{N} \\
 = & \frac{\delta_{ij}}{\zeta} \left(\int_X (\cdot) \nabla_{y_i}^2 g(x, y_i) w_i E_i(x) d\mu(x) \right. \\
 & \left. + \int_X (\cdot) (\nabla_{y_i} g(x, y_i))^2 w_i E_i(x) d\mu(x), \right. \\
 & \left. \delta_{ik} \int_X \nabla_{y_i}^2 g(x, y_i) w_i E_i(x) d\mu(x) \right. \\
 & \left. + \int_X (\nabla_{y_i} g(x, y_i))^2 w_i E_i(x) d\mu(x) \right), \tag{42}
 \end{aligned}$$

where in the last one, k represent the k -th component in \mathcal{N} 's second part (about $\bar{\beta}$).

C. Empirical Parts

C.1. Estimate $W_{k, \zeta}^k$: Richardson Extrapolation and Others

In the analysis, we may need $W_{k, \zeta}^k(\mu, \mu_m)$ to compare how discretization methods behave. However, when the μ is not discrete, generally we are not able to obtain the analytical solution to the Wasserstein distance.

In certain cases including all examples this paper contains, the Wasserstein can be estimated by finite samples (with a large size). According to (Mensch & Peyré, 2020), for $\mu \in \mathcal{P}(X)$ in our setup (a probability measure on a compact Polish space with Borel algebra) and $g = d_X^k \in \mathcal{C}(X^2)$ being a continuous function, the the Online Sinkhorn methods can be used to estimate $W_{k, \zeta}^k$. Online Sinkhorn needs a large number of samples for μ (in batch) to be accurate.

In our paper, as X are compact subsets in \mathbb{R}^n and μ has a continuous probability density function, we may use

Richardson Extrapolation method to estimate the Wasserstein distance between μ and μ_m , which may require fewer samples and fewer computations (Sinkhorn twice with different sizes).

Our examples are on intervals or rectangles, in which two grids Λ_1 of N points and Λ_2 of rN points (N and rN are both integers) can be constructed naturally for each. With μ determined by a smooth probability density function ρ , let $\mu_{(N)}$ be normalization of $\sum_{i=1}^N \rho(\Lambda_i) \delta_{\Lambda_i}$ (this may not be a probability distribution, so we use its normalization). From continuity of ρ and the boundedness of dual variables α, β , we can conclude that

$$\lim_{N \rightarrow \infty} W_{k,\zeta}^k(\mu_{(N)}, \mu_m) = W_{k,\zeta}^k(\mu, \mu_m).$$

Let $W_{k,\zeta}^k(\mu_{(N)}, \mu_m)$ be a function of $1/N$, to apply Richardson extrapolation, we need the exponent of lowest term of $1/N$ in the expansion $W_{k,\zeta}^k(\mu_{(N)}, \mu_m) = W^* + \mathcal{O}(1/N^h) + \mathcal{O}((1/N)^{h+1})$, where $W^* = W_{k,\zeta}^k(\mu, \mu_m)$.

Consider that

$$|W_{k,\zeta}^k(\mu, \mu_m) - W_{k,\zeta}^k(\mu_{(N)}, \mu_m)| \leq W_{k,\zeta}^k(\mu, \mu_{(N)})$$

Since $W_{k,\zeta}^k(\mu_{(N)}, \mu) \propto N^{-1/d}$, we may conclude that $h = k/d$, where d is the dimension of X . Figure 9 shows an empirical example in $d = 1, k = 2$ situation.

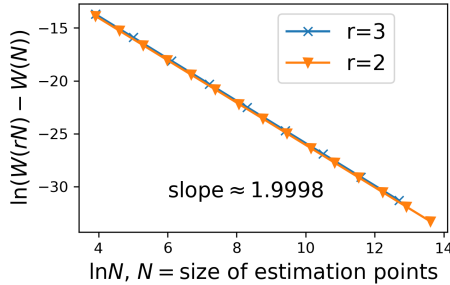


Figure 9. Richardson Extrapolation: the power of the expansion about N^{-1} . We take the EDOT μ_5 of example 2 (1-dim truncated normal mixture) as the target μ_m , use evenly positioned μ_N for different N 's to estimate. The y -axis is $\ln(W_{2,0.01}^2(\mu_{(rN)}, \mu_5) - W_{2,0.01}^2(\mu_{(N)}, \mu_5))$, where $r = 2$ and $r = 3$ are calculated. With $\ln N$ as x -axis, linearity can be observed. The slopes are both about -1.9998 , representing the exponent of the leading non-constant term of $W_{2,0.01}^2(\mu_{(N)}, \mu_5)$ on N , while the theoretical result is $r = -k/d = -2$. The differences are from higher order terms on N .

C.2. Example: The Sphere

The CW-complex structure of the unit sphere S^2 is constructed as: let $(1, 0, 0)$, the point on the equator be the only dimension-0 structure, and let the equator be the

dimension-1 structure (line segment $[0, 1]$ attached to the dimension-0 structure by identifying both end points to the only point $(1, 0, 0)$). The dimension-2 structure is the union of two unit discs, identified to the south / north hemisphere of S^2 by stereographic projection

$$\pi_{\pm N} : (X, Y) \rightarrow \frac{1}{1 + X^2 + Y^2} (2X, 2Y, \pm(X^2 + Y^2 - 1)) \quad (43)$$

with respect to the north / south pole.

Spherical Geometry. The spherical geometry is the Riemannian manifold structure induced by the embedding onto the unit sphere in \mathbb{R}^3 .

The geodesic between two points is the shorter arc along the great circle determined by the two points. In their \mathbb{R}^3 coordinates, $d_{S^2}(\mathbf{x}, \mathbf{y}) = \arccos(\langle \mathbf{x}, \mathbf{y} \rangle)$. Composed with stereographic projections, the distance in terms of CW-complex coordinates can be calculated (and be differentiated).

The gradient about \mathbf{y} (or its CW-coordinate) can be calculated via above formulas. In practice, the only problem is that when $\mathbf{x} = \pm \mathbf{y}$ function \arccos at ± 1 is singular. From the symmetry of sphere on the rotation along axis \mathbf{x} , the derivatives of distance along all directions are the same. Therefore, we may choose the radial direction on the CW-coordinate (unit disc). And the differentiations are primary to calculate.

C.3. A Note on the Implementation of SGD with Momentum

There is a slight difference between our implementation of the SGD and the Algorithm provided in the paper. In the implementation, we give two different learning rates to the positions (y_i 's) and the weights (w_i 's), as moving along positions is usually observed much slower than moving along weights. Empirically, we make the learning rates on position be exactly 3 times of the learning rates on weights, at each SGD iteration. With this change, the convergence is faster, but we do not have a theory or empirical evidences to show a fixed ratio 3 is the best choice.

Implementing and testing the Newton's method (hybrid with SGD) and other improved SGD methods could be good problems to work on.

C.4. Some Figures from Empirical Results

In this part, we post some figures revealing the results from the simulations, mainly the 3d figures in different directions.

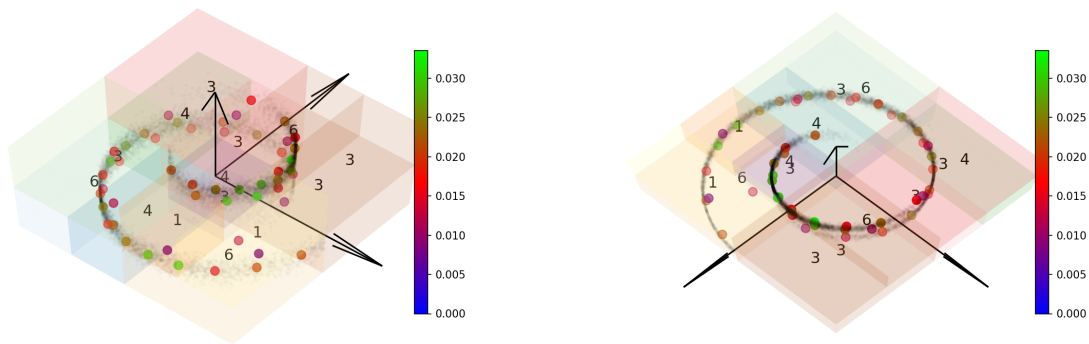


Figure 10. The Swiss roll example, 3D discretization (same as the paper) in different view directions.

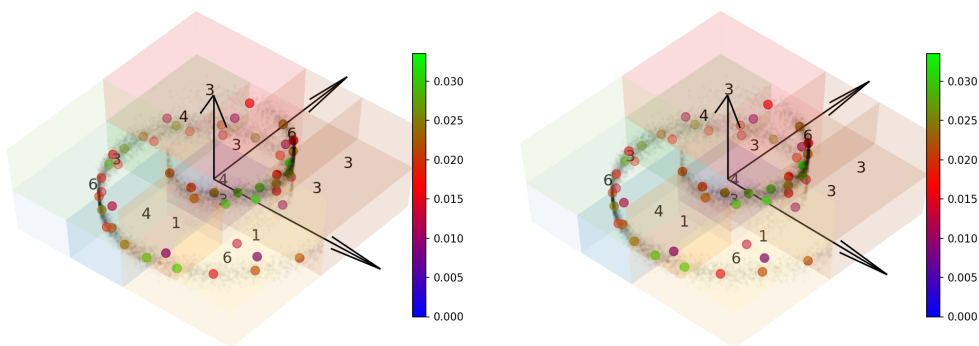


Figure 11. The Swiss roll example, 3D discretization (same as the paper) in terms of an autostereogram.

References

- Accinelli, E. A generalization of the implicit function theorems. Available at SSRN 1512763, 2009.
- Allen-Zhu, Z., Li, Y., Oliveira, R., and Wigderson, A. Much faster algorithms for matrix scaling. In *2017 IEEE 58th Annual Symposium on Foundations of Computer Science (FOCS)*, pp. 890–901. IEEE, 2017.
- Aude, G., Cuturi, M., Peyré, G., and Bach, F. Stochastic optimization for large-scale optimal transport. *arXiv preprint arXiv:1605.08527*, 2016.
- Cuturi, M. Sinkhorn distances: Lightspeed computation of optimal transport. In *Advances in neural information processing systems*, pp. 2292–2300, 2013.
- Dudley, R. M. The speed of mean glivenko-cantelli convergence. *The Annals of Mathematical Statistics*, 40(1): 40–50, 1969.
- Genevay, A., Chizat, L., Bach, F., Cuturi, M., and Peyré, G. Sample complexity of sinkhorn divergences. In *The 22nd International Conference on Artificial Intelligence and Statistics*, pp. 1574–1583. PMLR, 2019.
- Janati, H., Muzellec, B., Peyré, G., and Cuturi, M. Entropic optimal transport between unbalanced gaussian measures has a closed form. *Advances in Neural Information Processing Systems*, 33, 2020.
- Kantorovich, L. V. On the translocation of masses. *Journal of Mathematical Sciences*, 133(4):1381–1382, 2006.
- Lin, T., Ho, N., and Jordan, M. I. On the efficiency of the sinkhorn and greenhorn algorithms and their acceleration for optimal transport. *arXiv preprint arXiv:1906.01437*, 2019.
- Luise, G., Rudi, A., Pontil, M., and Ciliberto, C. Differential properties of sinkhorn approximation for learning with

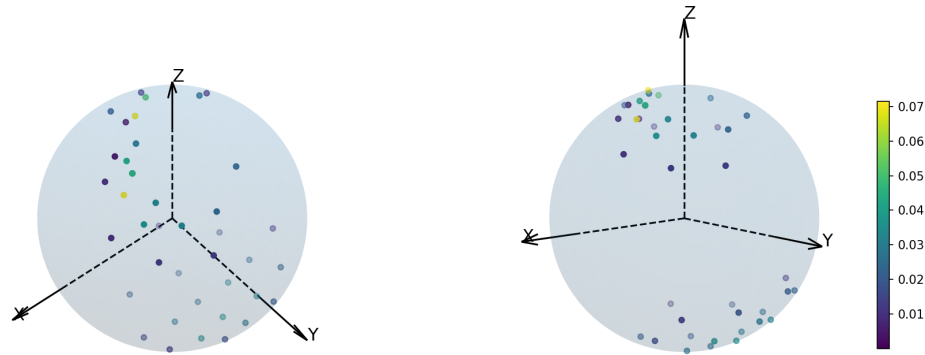


Figure 12. The Sphere example, 3D discretization (same as the paper) on two view directions.

wasserstein distance. In *Advances in Neural Information Processing Systems*, pp. 5859–5870, 2018.

Mensch, A. and Peyré, G. Online sinkhorn: Optimal transport distances from sample streams. *arXiv e-prints*, pp. arXiv–2003, 2020.

Overstall, A., McGree, J., et al. Bayesian design of experiments for intractable likelihood models using coupled auxiliary models and multivariate emulation. *Bayesian Analysis*, 15(1):103–131, 2020.

Peyré, G. and Cuturi, M. Computational optimal transport. *Foundations and Trends in Machine Learning*, 11(5-6): 355–607, 2019.

Sinkhorn, R. and Knopp, P. Concerning nonnegative matrices and doubly stochastic matrices. *Pacific Journal of Mathematics*, 21(2):343–348, 1967.

Tran, M.-N., Nott, D. J., and Kohn, R. Variational bayes with intractable likelihood. *Journal of Computational and Graphical Statistics*, 26(4):873–882, 2017.

Villani, C. *Optimal transport: old and new*, volume 338. Springer Science & Business Media, 2008.

Wang, J., Wang, P., and Shafto, P. Sequential cooperative bayesian inference. In *International Conference on Machine Learning*, pp. 10039–10049. PMLR, 2020a.

Wang, P., Wang, J., Paranamana, P., and Shafto, P. A mathematical theory of cooperative communication. *Advances in Neural Information Processing Systems*, 33, 2020b.

Weed, J., Bach, F., et al. Sharp asymptotic and finite-sample rates of convergence of empirical measures in wasserstein distance. *Bernoulli*, 25(4A):2620–2648, 2019.

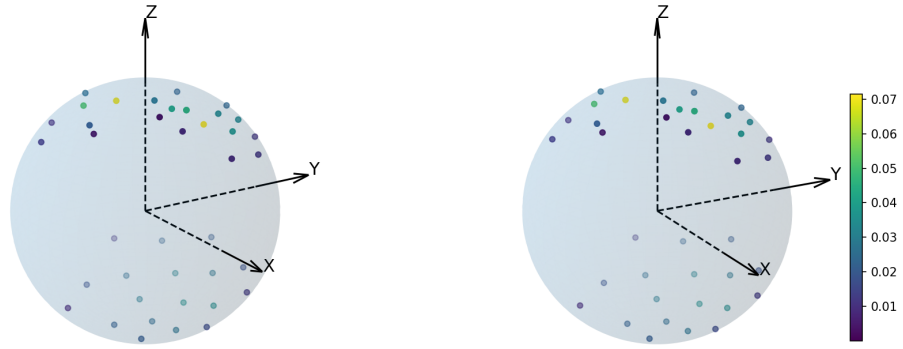


Figure 13. The Sphere example, 3D discretization (same as the paper) in terms of an autostereogram.

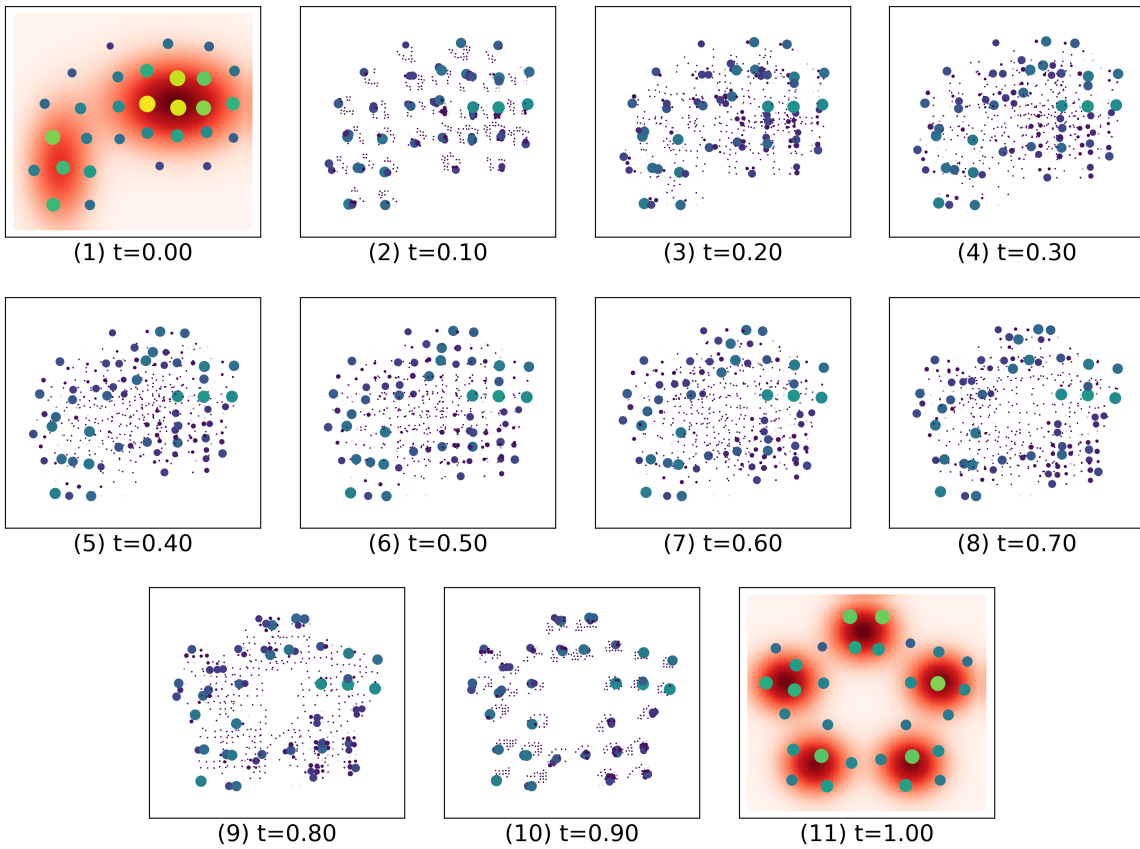


Figure 14. The McCann Interpolation figures in finer time resolution, for visualizing the transference plan from (1) to (11). It is a refined figure of the original paper. We see can see that the larger bubbles (representing a large probability mass) moves in a short distance and smaller pieces moves longer.